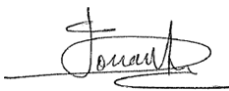# esa

SLBC_CCI+

SEA LEVEL BUDGET CLOSURE - CLIMATE CHANGE INITIATIVE +

UNCERTAINTY CHARACTERISATION REPORT (UCR)

	Name	Organisation	Date	Visa
Written by :	Martin Horwath Thorben Döhne	TU Dresden	31/03/2025	
	Robin Fraudeau Marie Bouih Ramiro Ferrari Michael Ablain	Magellium		
	Erwan Oulhen William Llovel Nicolas Kolodziejczyk Kevin Balem	LOPS		
	Hugo Lecomte Benoit Meyssignac Anny Cazenave Alejandro Blazquez Sébastien Fourest	LEGOS		
	Jonathan Bamber Anrijs Abele Xueqing Yin	Univ. Bristol		
	Giorgio Spada	UNIBO		

	Stéphanie Leroux	Datlas		
Checked by :	Michaël Ablain	Magellium	31/03/2025	
Approved by :	Joël Dorandeu	Magellium	31/03/2025	
Accepted by :	Sarah Connors	ESA		

Document reference:	SLBC_CCI-DT-076-MAG_UCR_D3-5
Edition.Revision:	1.0
Release date:	31/03/2025
Customer:	ESA
Ref. Market, consultation:	ESA AO/1-11340/22/I-NB

Mailing list

	Name	**organisation**	**Nb. copies**
Recipients :	Sarah Connors	ESA	1 digital copy
Internal copy :			1 digital copy

Document evolution sheet

Ed.	Rev.	Date	Purpose of evolution	Observations
1	0	31/03/2025	First version of the document	

Contents

List of figures and tables

1. Introduction

1.1. Scope and objective

This document is the Uncertainty Characterisation Report (UCR) of the ESA Sea Level Budget Close of the Climate Change Initiative+ (SLBC_cci+) project. This UCR is dedicated to the description of the uncertainties provided for every component of the SLB as well as the uncertainty assessment of the budget.

1.2. Document structure

In addition to this introduction, the document is organised as follows:

- Section 2 describes the scientific background of the project and the importance of the uncertainties characterisations
- Section 3 describes the uncertainties of each SLB component
- Section 4 presents the results of the uncertainties on the SLB regarding the historical approach (unconstrained)
- Section 5 presents the result of the uncertainties estimated for the innovative approach (objectively constrained)

1.3. Related documents

1.3.1. Applicable documents

Table 1 *List of applicable documents.*

Id.	Ref.	Description
[AD1]	SLBC_CCI-DT-075-MAG_PVIR	SEA LEVEL BUDGET CLOSURE_CCI+ Product Validation and Intercomparison Report
[AD2]	SLBC_CCI-DT-074-MAG_PUG	SEA LEVEL BUDGET CLOSURE_CCI+ Product User Guide
[AD3]	SLBC_CCI-DT-041-MAG_ATBD	SEA LEVEL BUDGET CLOSURE_CCI+ Algorithm Theoretical Baseline Document
[AD4]	SLBC_CCI-DT-039-MAG_PSD	SEA LEVEL BUDGET CLOSURE_CCI+ Product Specification Document
[AD5]	SLBC_CCI-DT-040-MAG_DARD	SEA LEVEL BUDGET CLOSURE_CCI+ Data Access Requirements Document
[AD6]	MAG-22-PTF-060_DetailedProposal_V2	Detailed proposal in response to ESA/ESRIN Request for Quotation "SEA LEVEL BUDGET

		CLOSURE_CCI+ (SLBC_CCI+)" AO/1-11340/22/I-NB	ESA

1.3.2. References

- A, G., Wahr, J., and Zhong, S.: Computations of the viscoelastic response of a 3-D compressible Earth to surface loading: an application to Glacial Isostatic Adjustment in Antarctica and Canada, Geophys. J. Int., 192, 557–572, https://doi.org/10.1093/gji/ggs030, 2013.
- Ablain, M., Meyssignac, B., Zawadzki, L., Jugier, R., Ribes, A., Spada, G., Benveniste, J., Cazenave, A., and Picot, N.: Uncertainty in satellite estimates of global mean sea-level changes, trend and acceleration, Earth Syst. Sci. Data, 11, 1189–1202, https://doi.org/10.5194/essd-11-1189-2019, 2019.
- Argus, D. F., Peltier, W. R., Drummond, R., and Moore, A. W.: The Antarctica component of postglacial rebound model ICE-6G_C (VM5a) based on GPS positioning, exposure age dating of ice thicknesses, and relative sea level histories, Geophys. J. Int., 198, 537–563, https://doi.org/10.1093/gji/ggu140, 2014.
- Barnoud, A., Pfeffer, J., Guérou, A., Frery, M., Siméon, M., Cazenave, A., Chen, J., Llovel, W., Thierry, V., Legeais, J., and Ablain, M.: Contributions of Altimetry and Argo to Non‑Closure of the Global Mean Sea Level Budget Since 2016, Geophys. Res. Lett., 48, e2021GL092824, https://doi.org/10.1029/2021GL092824, 2021.
- Barnoud, A., Picard, B., Meyssignac, B., Marti, F., Ablain, M., and Roca, R.: Reducing the Uncertainty in the Satellite Altimetry Estimates of Global Mean Sea Level Trends Using Highly Stable Water Vapor Climate Data Records, J. Geophys. Res. Oceans, 128, e2022JC019378, https://doi.org/10.1029/2022JC019378, 2023a.
- Barnoud, A., Pfeffer, J., Cazenave, A., Fraudeau, R., Rousseau, V., and Ablain, M.: Revisiting the global mean ocean mass budget over 2005–2020, Ocean Sci., 19, 321–334, https://doi.org/10.5194/os-19-321-2023, 2023b.
- Bloßfeld, M., Müller, H., Gerstl, M., Štefka, V., Bouman, J., Göttl, F., and Horwath, M.: Second-degree Stokes coefficients from multi-satellite SLR, J. Geod., 89, 857–871, https://doi.org/10.1007/s00190-015-0819-z, 2015.
- Brown, S., Willis, J., and Fournier, S.: Jason-3 Wet Path Delay Correction (Ver. F. PO.DAAC), https://doi.org/10.5067/J3L2G-PDCOR, 2023.
- Bruinsma, S., Lemoine, J.-M., Biancale, R., and Valès, N.: CNES/GRGS 10-day gravity field models (release 2) and their evaluation, Adv. Space Res., 45, 587–601, https://doi.org/10.1016/j.asr.2009.10.012, 2010.
- Cáceres, D., Marzeion, B., Malles, J. H., Gutknecht, B. D., Schmied, H. M., and Döll, P.: Assessing global water mass transfers from continents to oceans over the period 1948–2016, Hydrol. Earth Syst. Sci., 24, 4831–4851, https://doi.org/10.5194/hess-24-4831-2020, 2020.
- Camargo, C. M. L., Riva, R. E. M., Hermans, T. H. J., Schütt, E. M., Marcos, M., Hernandez-Carrasco, I., and Slangen, A. B. A.: Regionalizing the sea-level budget with machine learning techniques, Ocean Sci., 19, 17–41, https://doi.org/10.5194/os-19-17-2023, 2023.
- Caron, L., Ivins, E. R., Larour, E., Adhikari, S., Nilsson, J., and Blewitt, G.: GIA Model Statistics for GRACE Hydrology, Cryosphere, and Ocean Science, Geophys. Res. Lett., 45, 2203–2212, https://doi.org/10.1002/2017GL076644, 2018.
- Cazenave, A., Meyssignac, B., Ablain, M., Balmaseda, M., Bamber, J., Barletta, V., Beckley, B., Benveniste, J., Berthier, E., Blazquez, A., Boyer, T., Cáceres, D., Chambers,

D., Champollion, N., Chao, B., Chen, J., Cheng, L., Church, J. A., Chuter, S., Cogley, J. G., Dangendorf, S., Desbruyères, D., Döll, P., Domingues, C., Falk, U., Famiglietti, J., Fenoglio-Marc, L., Forsberg, R., Galassi, G., Gardner, A., Groh, A., Hamlington, B., Hogg, A., Horwath, M., Humphrey, V., Husson, L., Ishii, M., Jäggi, A., Jevrejeva, S., Johnson, G. C., Kolodziejczyk, N., Kusche, J., Lambeck, K., Landerer, F., Leclercq, P. W., Legresy, B., Leuliette, E., Llovel, W., Longuevergne, L., Loomis, B. D., Luthcke, S. B., Marcos, M., Marzeion, B., Merchant, C., Merrifield, M., Milne, G., Mitchum, G., Mohajerani, Y., Monier, M., Monselesan, D., Nerem, S., Palanisamy, H., Paul, F., Perez, B., Piecuch, C. G., Ponte, R. M., Purkey, S. G., Reager, J. T., Rietbroek, R., Rignot, E., Riva, R., Roemmich, D., Sørensen, L. S., Sasgen, I., Schrama, E. J. O., Seneviratne, S. I., Shum, C. K., Spada, G., Stammer, D., Velicogna, I., Von Schuckmann, K., Wada, Y., Wang, Y., Watson, C., Wiese, D., Wijffels, S., Westaway, R., Woppelmann, G., and Wouters, B.: Global sea-level budget 1993-present, https://doi.org/10.3929/ETHZ-B-000287786, 2018.

- Chen, J., Tapley, B., Seo, K.-W., Wilson, C., and Ries, J.: Improved Quantification of Global Mean Ocean Mass Change Using GRACE Satellite Gravimetry Measurements, Geophys. Res. Lett., 46, 13984–13991, https://doi.org/10.1029/2019GL085519, 2019.

- Chen, J., Cazenave, A., Dahle, C., Llovel, W., Panet, I., Pfeffer, J., and Moreira, L.: Applications and Challenges of GRACE and GRACE Follow-On Satellite Gravimetry, Surv. Geophys., https://doi.org/10.1007/s10712-021-09685-x, 2022.

- Cheng, M. and Ries, J.: C20 and C30 Variations From SLR for GRACE/GRACE-FO Science Applications, J. Geophys. Res. Solid Earth, 128, e2022JB025459, https://doi.org/10.1029/2022JB025459, 2023.

- Cheng, M., Tapley, B. D., and Ries, J. C.: Deceleration in the Earth's oblateness, J. Geophys. Res. Solid Earth, 118, 740–747, https://doi.org/10.1002/jgrb.50058, 2013.

- Dieng, H. B., Cazenave, A., Meyssignac, B., and Ablain, M.: New estimate of the current rate of sea level rise from a sea level budget approach, Geophys. Res. Lett., 44, 3744–3751, https://doi.org/10.1002/2017gl073308, 2017.

- Dussaillant, I., Hugonnet, R., Huss, M., Berthier, E., Bannwart, J., Paul, F., and Zemp, M.: Annual mass changes for each glacier in the world from 1976 to 2023, Earth Syst. Sci. Data Discuss., 1–41, https://doi.org/10.5194/essd-2024-323, 2024.

- Frederikse, T., Riva, R., Kleinherenbrink, M., Wada, Y., van den Broeke, M., and Marzeion, B.: Closing the sea level budget on a regional scale: Trends and variability on the Northwestern European continental shelf, Geophys. Res. Lett., 43, 10,864-10,872, https://doi.org/10.1002/2016GL070750, 2016.

- Frederikse, T., Jevrejeva, S., Riva, R. E. M., and Dangendorf, S.: A Consistent Sea-Level Reconstruction and Its Budget on Basin and Global Scales over 1958–2014, J. Clim., 31, 1267–1280, https://doi.org/10.1175/jcli-d-17-0502.1, 2018.

- Frederikse, T., Landerer, F., Caron, L., Adhikari, S., Parkes, D., Humphrey, V. W., Dangendorf, S., Hogarth, P., Zanna, L., Cheng, L., and Wu, Y.-H.: The causes of sea-level rise since 1900, Nature, 584, 393–397, https://doi.org/10.1038/s41586-020-2591-3, 2020.

- Good, S. A., Martin, M. J., and Rayner, N. A.: EN4: Quality controlled ocean temperature and salinity profiles and monthly objective analyses with uncertainty estimates, J. Geophys. Res. Oceans, 118, 6704–6716, https://doi.org/10.1002/2013JC009067, 2013.

- Groh, A. and Horwath, M.: Antarctic Ice Mass Change Products from GRACE/GRACE-FO Using Tailored Sensitivity Kernels, Remote Sens., 13, 1736, https://doi.org/10.3390/rs13091736, 2021.

- Guérou, A., Meyssignac, B., Prandi, P., Ablain, M., Ribes, A., and Bignalet-Cazalet, F.:

Current observed global mean sea level rise and acceleration estimated from satellite altimetry and the associated measurement uncertainty, Ocean Sci., 19, 431–451, https://doi.org/10.5194/os-19-431-2023, 2023.

- Hamlington, B. D., Frederikse, T., Nerem, R. S., Fasullo, J. T., and Adhikari, S.: Investigating the Acceleration of Regional Sea Level Rise During the Satellite Altimeter Era, Geophys. Res. Lett., 47, https://doi.org/10.1029/2019GL086528, 2020.

- Horwath, M., Gutknecht, B. D., Cazenave, A., Palanisamy, H. K., Marti, F., Marzeion, B., Paul, F., Bris, R. L., Hogg, A. E., Otosaka, I., Shepherd, A., Döll, P., Cáceres, D., Schmied, H. M., Johannessen, J. A., Nilsen, J. E. Ø., Raj, R. P., Forsberg, R., Sørensen, L. S., Barletta, V. R., Simonsen, S. B., Knudsen, P., Andersen, O. B., Randall, H., Rose, S. K., Merchant, C. J., Macintosh, C. R., Schuckmann, K. von, Novotny, K., Groh, A., Restano, M., and Benveniste, J.: Global sea-level budget and ocean-mass budget, with focus on advanced data products and uncertainty characterisation, Earth Syst. Sci. Data, 14, 411–447, https://doi.org/10.5194/essd-14-411-2022, 2022.

- Hugonnet, R., McNabb, R., Berthier, E., Menounos, B., Nuth, C., Girod, L., Farinotti, D., Huss, M., Dussaillant, I., Brun, F., and Kääb, A.: Accelerated global glacier mass loss in the early twenty-first century, Nature, 592, 726–731, https://doi.org/10.1038/s41586-021-03436-z, 2021.

- Kappelsberger, M. T., Strößenreuther, U., Scheinert, M., Horwath, M., Groh, A., Knöfel, C., Lunz, S., and Khan, S. A.: Modeled and Observed Bedrock Displacements in North-East Greenland Using Refined Estimates of Present-Day Ice-Mass Changes and Densified GNSS Measurements, J. Geophys. Res. Earth Surf., 126, e2020JF005860, https://doi.org/10.1029/2020JF005860, 2021.

- König, R., Schreiner, P., and Dahle, C.: Monthly estimates of C(2,0) generated by GFZ from SLR satellites based on GFZ GRACE/GRACE-FO RL06 background models (1.0), https://doi.org/10.5880/GFZ.GRAVIS_06_C20_SLR, 2019.

- Loomis, B. D., Rachlin, K. E., Wiese, D. N., Landerer, F. W., and Luthcke, S. B.: Replacing GRACE/GRACE-FO With Satellite Laser Ranging: Impacts on Antarctic Ice Sheet Mass Change, Geophys. Res. Lett., 47, e2019GL085488, https://doi.org/10.1029/2019GL085488, 2020.

- Ludwigsen, C. B., Andersen, O. B., Marzeion, B., Malles, J.-H., Müller Schmied, H., Döll, P., Watson, C., and King, M. A.: Global and regional ocean mass budget closure since 2003, Nat. Commun., 15, 1416, https://doi.org/10.1038/s41467-024-45726-w, 2024.

- Malles, J.-H. and Marzeion, B.: Twentieth century global glacier mass change: an ensemble-based model reconstruction, The Cryosphere, 15, 3135–3157, https://doi.org/10.5194/tc-15-3135-2021, 2021.

- Mu, Q., Müller, J., Wu, H., Knabe, A., and Zhong, M.: Satellite gradiometry based on a new generation of accelerometers and its potential contribution to Earth gravity field determination, Adv. Space Res., 73, 3321–3344, https://doi.org/10.1016/j.asr.2023.08.023, 2024.

- Müller Schmied, H., Trautmann, T., Ackermann, S., Cáceres, D., Flörke, M., Gerdener, H., Kynast, E., Peiris, T. A., Schiebener, L., Schumacher, M., and Döll, P.: The global water resources and use model WaterGAP v2.2e: description and evaluation of modifications and new features, Geosci. Model Dev., 17, 8817–8852, https://doi.org/10.5194/gmd-17-8817-2024, 2024.

- Nerem, R. S., Beckley, B. D., Fasullo, J. T., Hamlington, B. D., Masters, D., and Mitchum, G. T.: Climate-change–driven accelerated sea-level rise detected in the altimeter era, Proc.

Natl. Acad. Sci., 201717312, https://doi.org/10.1073/pnas.1717312115, 2018.

- Nilsson, J. and Gardner, A. S.: Elevation Change of the Greenland Ice Sheet and its Peripheral Glaciers: 1992–2023, Earth Syst. Sci. Data Discuss., 1–28, https://doi.org/10.5194/essd-2024-311, 2024.
- Nilsson, J., Gardner, A. S., and Paolo, F. S.: Elevation change of the Antarctic Ice Sheet: 1985 to 2020, Earth Syst. Sci. Data, 14, 3573–3598, https://doi.org/10.5194/essd-14-3573-2022, 2022.
- Otosaka, I. N., Shepherd, A., Ivins, E. R., Schlegel, N.-J., Amory, C., van den Broeke, M. R., Horwath, M., Joughin, I., King, M. D., Krinner, G., Nowicki, S., Payne, A. J., Rignot, E., Scambos, T., Simon, K. M., Smith, B. E., Sørensen, L. S., Velicogna, I., Whitehouse, P. L., A, G., Agosta, C., Ahlstrøm, A. P., Blazquez, A., Colgan, W., Engdahl, M. E., Fettweis, X., Forsberg, R., Gallée, H., Gardner, A., Gilbert, L., Gourmelen, N., Groh, A., Gunter, B. C., Harig, C., Helm, V., Khan, S. A., Kittel, C., Konrad, H., Langen, P. L., Lecavalier, B. S., Liang, C.-C., Loomis, B. D., McMillan, M., Melini, D., Mernild, S. H., Mottram, R., Mouginot, J., Nilsson, J., Noël, B., Pattle, M. E., Peltier, W. R., Pie, N., Roca, M., Sasgen, I., Save, H. V., Seo, K.-W., Scheuchl, B., Schrama, E. J. O., Schröder, L., Simonsen, S. B., Slater, T., Spada, G., Sutterley, T. C., Vishwakarma, B. D., van Wessem, J. M., Wiese, D., van der Wal, W., and Wouters, B.: Mass balance of the Greenland and Antarctic ice sheets from 1992 to 2020, Earth Syst. Sci. Data, 15, 1597–1616, https://doi.org/10.5194/essd-15-1597-2023, 2023.
- Peltier, W. R., Argus, D. F., and Drummond, R.: Space geodesy constrains ice age terminal deglaciation: The global ICE-6G_C (VM5a) model, J. Geophys. Res. Solid Earth, 120, 450–487, https://doi.org/10.1002/2014JB011176, 2015.
- Peltier, W. R., Argus, D. F., and Drummond, R.: Comment on "An Assessment of the ICE-6G_C (VM5a) Glacial Isostatic Adjustment Model" by Purcell et al., J. Geophys. Res. Solid Earth, 123, 2019–2028, https://doi.org/10.1002/2016JB013844, 2018.
- Prandi, P., Meyssignac, B., Ablain, M., Spada, G., and Ribes, A.: Error variance-covariance, trends, accelerations and uncertainties of regional mean sea level estimated from satellite altimetry, https://doi.org/10.17882/74862, 2020.
- Prandi, P., Meyssignac, B., Ablain, M., Spada, G., Ribes, A., and Benveniste, J.: Local sea level trends, accelerations and uncertainties over 1993–2019, Sci. Data, 8, 1, https://doi.org/10.1038/s41597-020-00786-7, 2021.
- Rietbroek, R., Brunnabend, S.-E., Kusche, J., Schröter, J., and Dahle, C.: Revisiting the contemporary sea-level budget on global and regional scales, Proc. Natl. Acad. Sci., 113, 1504–1509, https://doi.org/10.1073/pnas.1519132113, 2016.
- Roquet, F., Madec, G., McDougall, T. J., and Barker, P. M.: Accurate polynomial expressions for the density and specific volume of seawater using the TEOS-10 standard, Ocean Model., 90, 29–43, https://doi.org/10.1016/j.ocemod.2015.04.002, 2015.
- Roy, K. and Peltier, W. R.: Glacial isostatic adjustment, relative sea level history and mantle viscosity: reconciling relative sea level model predictions for the U.S. East coast with geological constraints, Geophys. J. Int., 201, 1156–1181, https://doi.org/10.1093/gji/ggv066, 2015.
- Royston, S., Vishwakarma, B. D., Westaway, R., Rougier, J., Sha, Z., and Bamber, J.: Can We Resolve the Basin-Scale Sea Level Trend Budget From GRACE Ocean Mass?, J. Geophys. Res. Oceans, 125, https://doi.org/10.1029/2019jc015535, 2020.
- Shihora, L., Balidakis, K., Dill, R., Dahle, C., Ghobadi-Far, K., Bonin, J., and Dobslaw, H.: Non-Tidal Background Modeling for Satellite Gravimetry Based on Operational ECWMF

and ERA5 Reanalysis Data: AOD1B RL07, J. Geophys. Res. Solid Earth, 127, e2022JB024360, https://doi.org/10.1029/2022JB024360, 2022.

- Spada, G. and Melini, D.: SELEN[4] (SELEN version 4.0): a Fortran program for solving the gravitationally and topographically self-consistent sea-level equation in glacial isostatic adjustment modeling, Geosci. Model Dev., 12, 5055–5075, https://doi.org/10.5194/gmd-12-5055-2019, 2019.
- Sun, Y., Riva, R., and Ditmar, P.: Optimizing estimates of annual variations and trends in geocenter motion and J2 from a combination of GRACE data and geophysical models, J. Geophys. Res. Solid Earth, 121, 8352–8370, https://doi.org/10.1002/2016JB013073, 2016.
- Swenson, S., Chambers, D., and Wahr, J.: Estimating geocenter variations from a combination of GRACE and ocean model output, J. Geophys. Res. Solid Earth, 113, https://doi.org/10.1029/2007JB005338, 2008.
- Van Wessem, J. M., Van De Berg, W. J., Noël, B. P. Y., Van Meijgaard, E., Birnbaum, G., Jakobs, C. L., Krüger, K., Lenaerts, J. T. M., Lhermitte, S., Ligtenberg, S. R. M., Medley, B., Reijmer, C. H., Van Tricht, K., Trusel, L. D., Van Ulft, L. H., Wouters, B., Wuite, J., and Van Den Broeke, M. R.: Modelling the climate and surface mass balance of polar ice sheetsusing RACMO2, part 2: Antarctica (1979–2016), https://doi.org/10.5194/tc-2017-202, 9 October 2017.
- Veldhuijsen, S. B. M., van de Berg, W. J., Brils, M., Kuipers Munneke, P., and van den Broeke, M. R.: Characteristics of the 1979–2020 Antarctic firn layer simulated with IMAU-FDM v1.2A, The Cryosphere, 17, 1675–1696, https://doi.org/10.5194/tc-17-1675-2023, 2023.
- WCRP Global Sea Level Budget Group: Global sea-level budget 1993–present, Earth Syst. Sci. Data, 10, 1551–1590, https://doi.org/10.5194/essd-10-1551-2018, 2018.
- Wong, A. P. S., Wijffels, S. E., Riser, S. C., Pouliquen, S., Hosoda, S., Roemmich, D., Gilson, J., Johnson, G. C., Martini, K., Murphy, D. J., Scanderbeg, M., Bhaskar, T. V. S. U., Buck, J. J. H., Merceur, F., Carval, T., Maze, G., Cabanes, C., André, X., Poffa, N., Yashayaev, I., Barker, P. M., Guinehut, S., Belbéoch, M., Ignaszewski, M., Baringer, M. O., Schmid, C., Lyman, J. M., McTaggart, K. E., Purkey, S. G., Zilberman, N., Alkire, M. B., Swift, D., Owens, W. B., Jayne, S. R., Hersh, C., Robbins, P., West-Mack, D., Bahr, F., Yoshida, S., Sutton, P. J. H., Cancouët, R., Coatanoan, C., Dobbler, D., Juan, A. G., Gourrion, J., Kolodziejczyk, N., Bernard, V., Bourlès, B., Claustre, H., D'Ortenzio, F., Le Reste, S., Le Traon, P.-Y., Rannou, J.-P., Saout-Grit, C., Speich, S., Thierry, V., Verbrugge, N., Angel-Benavides, I. M., Klein, B., Notarstefano, G., Poulain, P.-M., Vélez-Belchí, P., Suga, T., Ando, K., Iwasaska, N., Kobayashi, T., Masuda, S., Oka, E., Sato, K., Nakamura, T., Sato, K., Takatsuki, Y., Yoshida, T., Cowley, R., Lovell, J. L., Oke, P. R., van Wijk, E. M., Carse, F., Donnelly, M., Gould, W. J., Gowers, K., King, B. A., Loch, S. G., Mowat, M., Turton, J., Rama Rao, E. P., Ravichandran, M., Freeland, H. J., Gaboury, I., Gilbert, D., Greenan, B. J. W., Ouellet, M., Ross, T., Tran, A., Dong, M., Liu, Z., Xu, J., Kang, K., Jo, H., et al.: Argo Data 1999–2019: Two Million Temperature-Salinity Profiles and Subsurface Velocity Observations From a Global Array of Profiling Floats, Front. Mar. Sci., 7, 2020.

1.4. Acronyms

Table 2 *List of abbreviations and acronyms.*

Acronyms	Description
C3S	Copernicus Climate Change Service
CCI	The ESA Climate Change Initiative
CDS	Climate Data Store
ECV	Essential Climate Variable
ERA5	ECMWF Atmospheric Reanalysis v5
ESA	European Space Agency
ECMWF	European Centre for Medium-range Weather Forecasts
GIA	Glacial Isostatic Adjustment
HOAPS	Hambourg Ocean-Atmosphere Fluxes and Parameters from Satellite
ISBA-CTRIP	Interaction Soil-Biosphere-Atmosphere, Total Runoff Integrating Pathways from the Centre National de Recherches Météorologiques
LWS	Land Water Storage
SLBC	Sea level budget closure
SLBC_cci	Sea Level Budget Closure of the ESA Climate Change Initiative (first phase)
SLBC_cci+	Sea Level Budget Closure of the ESA Climate Change Initiative (second phase, this activity)
SL_cci	The Sea Level component of the ESA Climate Change Initiative
TCWV	Total Column Water Vapour
TWS	Terrestrial Water Storage
WaterGAP	Water Global Assessment and Prognosis
WGHM	WaterGAP Hydrological Model
w.r.t	With respect to
WTC	Wet Troposphere Correction

2. Scientific Context

Assessing the sea level budget at global, regional, and local scales during the altimetry era—by comparing altimetry-based sea level time series with the sum of contributing components—is crucial for several reasons. It enables: 1) A better understanding of underlying processes of sea level rise, 2) Detection of temporal changes in one or more components (e.g., acceleration, abrupt

shifts) that contribute to sea level trends, 3) Identification and quantification of missing contributions if the budget does not close 4) Detection of systematic instrumental biases, drifts, or observational gaps, and 5) Validation of sea level models (e.g., reanalyses, coupled climate models) and their components.

At the global scale, sea level budget assessments have been the focus of extensive research (e.g., Dieng et al., 2017; Cazenave et al., 2018; Nerem et al., 2018; WCRP Global Sea Level Budget Group, 2018; Chen et al., 2019, 2022; Horwath et al., 2022; Barnoud et al., 2021, 2023). These studies generally agree that the global mean sea level budget closed within uncertainties up to around 2016 (also supported by IPCC 2019, 2021). However, more recent analyses (e.g., Chen et al., 2022; Barnoud et al., 2021, 2023; Mu et al., 2024) report a lack of closure thereafter, potentially due to instrumental issues such as radiometer drift on Jason-3 or accelerometer failure on GRACE/GRACE-FO missions. These findings underscore the critical need for ongoing comparisons between altimetry-based sea level data and the sum of individual contributions.

At the regional level, budget studies are comparatively fewer. Some recent efforts have evaluated closure at the basin or sub-basin scale during the altimetry period (e.g., Rietbroek et al., 2016; Frederikse et al., 2016, 2018, 2020; Hamlington et al., 2020; Royston et al., 2020; Camargo et al., 2023; Mu et al., 2024), and ocean mass budgets have also been studied regionally (e.g., Ludwigsen et al., 2024). However, closure is only achieved in certain regions. For example, Royston et al. (2020), using altimetry, gravimetry, and Argo data from 2005–2015, found the budget did not close in the Indian–South Pacific region. Similarly, Camargo et al. (2023) reported unresolved budgets in various ocean areas. Using machine learning techniques, these authors identified processes not adequately captured by current observations, contributing to the non-closure.

Re-examining the global and regional sea level budget using novel approaches is therefore essential. The first objective of this project is to extend the previous SLB and ocean mass budget (OMB) products at least until 2022 included, covering both altimetry era and GRACE/Argo era on a monthly time scale. For this new version, the impact on the SLB of CCI ECVs not previously considered are evaluated, as well as the inclusion of any ECV that significantly improves the closure. A key aspect of the sea level budget is the uncertainty budget as it fixes the level to which the budget is considered "closed within uncertainties". Accurate estimation of uncertainties is the unique method to identify dates and causes of SLB misclosure. This project proposes improved estimates of the uncertainties thanks to a better estimate of the individual components' uncertainties and an estimate of the systematic component of the SLB uncertainties related to the different time and space resolution of the different components of the observing systems including satellite altimetry space gravimetry and in-situ profilers. The second objective of this project is to apply the same approach to assess the closure of the SLB at regional scales. The last objective is to use the results at both global and regional scale to explain the time and space variability in SLB both at global and regional spatial scales.

3. Uncertainties estimations of each SLBC components

The objective of this section is to describe the measurement uncertainties of each SLB component which are the uncertainties associated with the instrumental error and the algorithmic approximations of each observing system that measures an individual contribution to sea level. It refers to the accuracy and precision of each individual subsystem within the SLB observing system. It provides a quantitative measure of how well each component performs and represents the uncertainty that can be reduced through improvements in instrumentation.

3.1. Altimetric component

The uncertainties of the altimetry-based global mean sea level are computed using the method and information from Ablain et al. (2019) and updated by Guérou et al. (2023). Table 3 summarises the sources of uncertainties for the global mean sea level and their estimates. For the uncertainty of the radiometer WTC, unlike in Guérou et al. (2023), the uncertainty is not increased over Jason-3 period as the Jason-3 WTC drift is corrected with the correction provided by Brown et al. (2023). The Glacial Isostatic Adjustment (GIA) contribution to the global mean sea level uncertainty is not applicable to the component not corrected for the GIA effect as described in this section, but this uncertainty contribution may be considered while no other estimate is available for the GIA component. Using the values in Table 3, the covariance matrix of the global mean sea level is computed following the method from Ablain et al. (2019).

Table 3 *Sources of uncertainties of the global mean sea level and their estimates, adapted from Guérou et al. (2023). Values in bold font have been updated since the estimates published by Guérou et al. (2023). In gray, the GIA contribution to sea level uncertainty is not applicable to the component not corrected for the GIA effect as described in this section, but this uncertainty contribution may be considered for any separate GIA component.*

Source of uncertainty	Type of uncertainty	Standard uncertainty u
Short-time correlated errors due to precise orbit determination (POD), altimeter parameters, geophysical corrections	Correlated effects with correlation duration of 2 months	**u = 1.6 mm for TP period** **u = 1.2 mm for J1 period** **u = 1.1 mm for J2 period** **u = 1.0 mm for J3 period** **u = 1.3 mm for S6MF period**
	Correlated effects with correlation duration of 1 year	**u = 1.2 mm for TP period** **u = 1.1 mm for J1 period** **u = 1.1 mm for J2 period** **u = 1.0 mm for J3 period** **u = 1.2 mm for S6MF period**
Radiometer WTC stability	Correlated errors with correlation	**u = 1.1 mm**

		duration of 5 years	
POD stability	Gravity fields	Correlated errors with correlation duration of 10 years	u = 1.12 mm for TP u = 0.5 mm for J1/J2/J3
	International Terrestrial Reference Frame (ITRF)	Linear time-correlated effect (also called "Drift")	u = 0.1 mm/yr
Inter-mission offsets		Offset	u = 2.0 mm for TPA/TPB **u = 0.6 mm for TP/J1** **u = 0.2 mm for J1/J2** **u = 0.2 mm for J2/J3** **u = 0.6 mm for J3/S6MF**
Global Isostatic Adjustment (GIA) correction		Linear time-correlated effect (also called "Drift")	u = 0.05 mm/yr
Altimeter parameters stability		Linear time-correlated effect (also called "Drift")	u = 0.7 mm/yr for TPA u = 0.1 mm/yr for TPB

The uncertainties linked to the gridded sea level anomaly data are described by Prandi et al. (2021). As for the global mean uncertainty budget, the GIA contribution to sea level uncertainty is not applicable to the component not corrected for the GIA effect as described in this section, but this uncertainty contribution may be considered while no other estimate is available for the GIA component. Table 4 summarises the sources of uncertainties for the local sea level change. Within each cell of 1°x1°, the covariance matrix of the local sea level change can be computed using the information from Table 4.

Table 4 *Sources of uncertainties of the sea level change and their estimates, from Prandi et al. (2021). Location dependent standard uncertainties are provided in the Prandi et al. (2020) dataset. In gray, the GIA contribution to sea level uncertainty is not applicable to the component not corrected for the GIA effect as described in this section, but this uncertainty contribution may be considered for any separate GIA component.*

Source of uncertainty	Type of error	Standard uncertainty u
Geophysical corrections and orbit determination	Correlated errors with correlation duration of 1 year	Location dependent, provided in Prandi et al. (2020)
Radiometer WTC	Correlated errors with correlation duration of 10 years	Location dependent, provided in Prandi et al. (2020)

Orbit determination	Drift	u = 0.33 mm/yr
GIA correction	Drift	Location dependent, provided in Prandi et al. (2020)
Inter-mission offsets	Offset	u = 10 mm for TPA/TPB and TPB/J1 u = 6 mm for J1/J2 and J2/J3

Known limitations

The vDT2021 version of C3S sea level anomaly data does not use the latest release of altimetry along-track data (vDT2024). For instance, the data from the latest reprocessing of TOPEX observations are not included yet.

Spatial correlations are not taken into account in the local sea level change uncertainties.

3.2. Steric component

Error in ISAS Optimal Interpolation :

The steric sea level component is determined through an analysis of Argo in situ profiles. This analysis is based on ISAS optimal interpolation (Gaillard et al., 2016). The uncertainty in the steric component is thus related to the analysis error of ISAS , which depends mainly of the a priori variance and the sampling of the in situ data, and to their instrumental error.

Analyzed Error covariance in ISAS: P^a, is determined by :

$$P^a = P^b - K\,C^{oa}$$

Where P^b is the a priori variance, i.e. the uncertainty in the absence of observations, characterized by interannual variability ; K is the Kalman gain, with $K = C^{ao}(C^{oo} + R)^{-1}$. It considers C^{ao}, the covariance between background field and observation, C^{oo} , the covariance of the observations, and R, the observational error matrix. In ISAS, the covariance matrices are functions of the distance between target grid points and observations, with decaying strength shaped by a correlation radius set as L1 = 300 km and a second spatially-varying radius (L2) about 4 time the first Rossby radius (latitudinal and bathymetrical depend). The zonal correlation radius is extended to 600 km in the Tropical band to account anisotropy of the tropical circulation. The magnitude of the covariance matrices are set a priori as the local interannual variance (temperature or salinity with removal of the monthly climatology): σ^2, with weighting depending on the scale considered (Gaillard et al., 2016):

$$\sigma^2_{L1} = W_1 \sigma^2 \; ; \; \sigma^2_{L2} = W_2 \sigma^2 \; ; \; \sigma^2_{RE} = W_3 \sigma^2 ,$$

where $W_1 + W_2 + W_3 = 1$, are the normalized weights, σ^2_{L1} and σ^2_{L2} are the variance associated with correlation radii L1 and L2, and σ^2_{RE} is the representativity error variance, associated to unresolved scales (see next Section). Prior to normalization, W_1, W_2, W_3 are respectively equal to 1, 2, and 8.

The final error in ISAS ($\sigma^a(x,t)$) is the square root of the diagonal of $P^a(x,t)$ Matrix at position $\vec{x}$ in three-dimensional space and time t.

Observational Error :

The observational error is determined by representativeness error (variability of the observed system not well resolved by the sampling of the observation data), instrumental error (precision and bias), and synoptic error (which occurs when measurements taken at different times may, for example, observe the same structure that has displaced). However, with the Argo floats, not all these errors have the same magnitude.

The representativeness error is set as the ⅛ of the local variance of the interannual anomalies (temperature or salinity whose monthly climatology is removed), estimated with a priori knowledge, i.e. past ISAS versions. Such definition allows considering the impact of mesoscale dynamics on Argo measurements.

The instrumental accuracy is about 0.002°C for temperature, 0.01 PSS-78 for salinity (Wong et al., 2020). In ISAS, only delayed profiles are analysed, so the risk to include bad quality measurements is reduced, as well as that of instrumental drift. The real-time quality control is a prior and automatic procedure, consisting of several tests to determine whether a measurement is spurious and to quantify its quality. For example, comparing the departure of an observation from the climatology with the expected standard deviation is a way of identifying abnormal anomalies. The Delayed Mode Quality Control (DMQC) is a second stage detection of spurious profiles by an expert. It aims at correcting drifts and biases that can affect Argo observations, due to sensor nominal drift or potential defects. These issues were addressed by identifying the importance of the drift and estimating a correction for the affected profiles.

The uncertainty in ISAS salinity (σ^a_S) and temperature (σ^a_T) fields reflect the sampling of the Argo floats. Overall, when they are absent, the a priori variance associated with interannual variability sets the uncertainty, and when observations are close, the uncertainty is reduced to the observational error.

Steric sea level error :

For estimating the error in steric sea level, the error in density (P_ρ^a) must be assessed. For that, several approximations of the thermal expansion coefficient and haline contraction coefficient are done. The former is approximated as $\alpha(\vec{x}, t) \approx 0.07 + 0.0137 \times T(x, t)$, where T is the temperature, and ß ≈ 0.75. This permits to consider the non-linearity in the density calculation (dependance of α to temperature, Roquet et al., 2015), while simplifying the calculation. The error of the density is thus : $\sigma_\rho(\vec{x}, t) = \sqrt{[\alpha(\vec{x}, t, T(x, t))\, \sigma_T^a(\vec{x}, t)]^2 + [\beta\, \sigma_S^a(\vec{x}, t)]^2}$.

Thus, when calculating the steric height error $\sigma_{SSL}^2(\vec{x}_{horizontal}, t)$, we have:

$$\sigma_{SSL}^2(\vec{x}_{horizontal}, t) = \sum_z \left[\frac{\Delta Z(z)\, \sigma_\rho(\vec{x}(z), t)}{\rho_0}\right]^2 + \sum_z \sum_{z_2 \neq z} \xi(\vec{x}(z), \vec{x}(z_2)) \left[\frac{\Delta Z(z)\, \sigma_\rho(\vec{x}(z), t)}{\rho_0}\right]\left[\frac{\Delta Z(z_2)\, \sigma_\rho(\vec{x}(z_2), t)}{\rho_0}\right] \quad ,$$

Where $\Delta Z(z)$ is the layer thickness at depth z, ρ_0 = 1026 kg m^{-3} is the surface seawater density, and $\xi(z, z_2)$ is the vertical covariance between to depth levels z and z_2. This temporal covariance is estimated using three-dimensional temperature ISAS analyses This calculation thus considers local uncertainty on density, but also the impact of errors at other levels.

Analysis of the uncertainty :

In figure … a, the mean uncertainty of the steric height estimate is shown. It reveals regions with more intense dynamics (Kuroshio Current, Antarctic Circumpolar Current…) and thus higher standard deviation (Figure …b) are associated with greater uncertainty (superior to 15mm). However, at the tropics, the correlation between uncertainty and the interannual standard deviation is reduced (Figure …a and b). There, the uncertainty is reduced. This is due to the presence of a greater amount of observations in the subtropics and tropics, as evidenced by a lower Pctvar (ranging in 25-50%) in these regions (Figure …c),

(a) Mean uncertainty
(b) Standard deviation
(c) Percent. Variance

| 0 | 15 | 30 |
Uncert. (mm)

| 0 | 60 | 120 |
STD. (mm)

| 0 | 25 | 50 | 75 | 100 |
Pctvar (%)
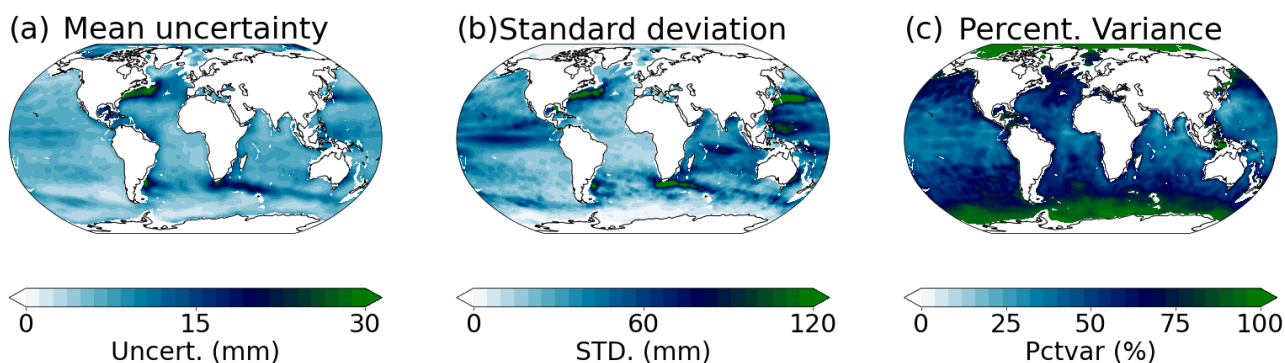
Figure: The temporally averaged (a) estimated steric height error, (b) interannual standard deviation of the steric height, and (c) 0-2000 m vertically averaged percentage of the variance (Pctvar). The Pctvar ranges from 0 to 100%, with lower values attained when local observations influence the analysis and higher values set as the default.

The influence of observations on reducing the uncertainty is clearly evidenced by their respective temporal evolution (figure …+1). Between 2005 and 2021, spatially averaged uncertainty diminishes from 8.5 mm to about 7.2, while the Pctvar is affected with similar changes, starting at about 80% and finishing at 65%.
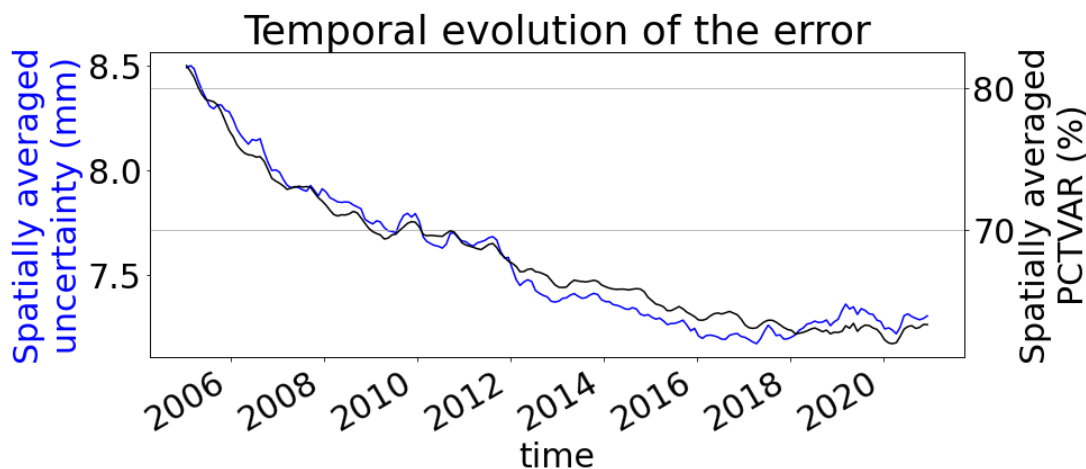
Figure: Spatially averaged estimated steric height error (in blue) and Pctvar (in black) evolutions with time.

3.3. Manometric and Barystatic component from GRACE

We assess time-dependent error variances and covariances of our time series of regionally integrated mass changes, such as the global ocean mass change. This includes a separate assessment of errors from the following error sources:

(a) uncorrelated noise propagated from the GRACE L2 solutions

(b) errors propagated from the low-degree harmonics (degree-one, C_{20})

(c) leakage errors

(d) errors of geophysical corrections, most importantly for GIA.

The methods to assess the individual error sources and to construct the related error covariance matrices are a refinement of the methods used by Groh and Horwath (2021), and we specify them in the following for error sources (a)-(d).

(a) We assess the uncorrelated-noise component of the mass time series by the RMS of a high-pass filtered time series, scaled with a factor that compensates for the attenuation of the RMS of white noise by the high-pass filtering. The steps of this method are illustrated in Figure 1 for the time series of the manometric estimate for the global ocean.

(b) We use ensembles of alternative low-degree harmonics time series and take the spread of the ensembles as an indication of their uncertainty. Particularly, we use the spread of linear trends of the ensemble members to assess the uncertainty propagated to the linear trend of the mass change time series. The degree-one ensemble includes nine time series and covers multiple methods, input data sets and background models used during the processing. It includes three time series provided in TN-13 (Sun et al., 2016; Swenson et al., 2008), four time series from our own implementation of the method by Sun et al. (2016), one time series of a combination approach by Rietbroek et al. (2016) and one time series derived from SLR measurements by Cheng et al. (2013). The C_{20} ensemble includes five time series derived from SLR measurements (Loomis et al., 2020; Cheng and Ries, 2023; Cheng et al., 2013; Bloßfeld et al., 2015; König et al., 2019), one time series from a combined analysis of SLR and GRACE (Bruinsma et al., 2010) and one time series based on GRACE (Sun et al., 2016). The ensembles for degree-one and C_{20} are illustrated by their contribution to the global ocean mass change estimate in Figure 2 a and b, respectively.

(c) We assess leakage errors by simulations, similarly to Groh and Horwath (2021), but with an updated and extended set of synthetic models. The simulations use synthetic signals of terrestrial water storage changes, glacier mass changes, ice-sheet mass changes, and ocean dynamics. For the ocean domain we use the oceanic component of release 07 of the Atmosphere and Ocean De-Aliasing Level-1B product (Shihora et al., 2022). For terrestrial water mass changes we use model output of the WaterGAP v2.2e model (Müller Schmied et al., 2024) and mask out grid cells covering Greenland. Mass changes of the Greenland and Antarctic ice sheets including peripheral glaciers are based on elevation changes measured by altimetry (Nilsson et al., 2022; Nilsson and Gardner, 2024). The elevation changes for Greenland and Antarctica are converted to mass changes using the density mask of Kappelsberger et al. (2021) and an ice density of 917 kgm^{-3} after accounting for changes of the firn air content using surface mass balance from the RACMO2.3p2 model (Van Wessem et al., 2017) and firn thickness change from the IMAU-FDM v1.2A model (Veldhuijsen et al., 2023). Global glacier mass changes are based on the model output of Malles and Marzeion (2021) after masking out grid cells covering Greenland. For each gridded dataset of mass changes, we derive sets of SH coefficients with n_{max} = 180 and amend them with their sea-level fingerprints to account for global mass redistribution. The synthetic signals are then converted to their gravity field effect in the SH domain. After SH truncation to the maximum SH degree of the GRACE L2 solutions, they are then processed in the same way as the GRACE L2 solutions are processed. The difference between the resulting simulated mass change solutions and the original synthetic mass change represent the simulated leakage effects. We consider the leakage effect as an autocorrelated stochastic process, and we consider the simulated leakage effects as a representation of this process. Our aim is to characterize this autocorrelated 'noise' by an analytical spectral model adjusted to the simulated leakage error time

series. As the simplest, and most relevant, component of auto-correlated noise we assess its temporally linear component from the linear components of the simulated leakage error time series. To increase the size of the ensemble and to make the spread more representative we calculate the linear component for every yearly interval between 9 and 12 years and estimate the leakage error uncertainty by computing the RMS over these linear components.

(d) We consider GIA, and hence GIA model errors, as strictly linear in time over the 23 years of GRACE/GRACE-FO. Following Horwath et al. (2022) we assess the uncertainty of the GIA corrections from the spread among an ensemble of alternative GIA corrections. The ensemble includes the ICE-6G_D model (Peltier et al., 2018), the ICE-5Gv2 model (A et al., 2013), the model by Caron et al. (2018) and the model from UNIBO used in this project. Time series of estimated mass changes of the global ocean using these different GIA model corrections are illustrated in Figure 2 c.
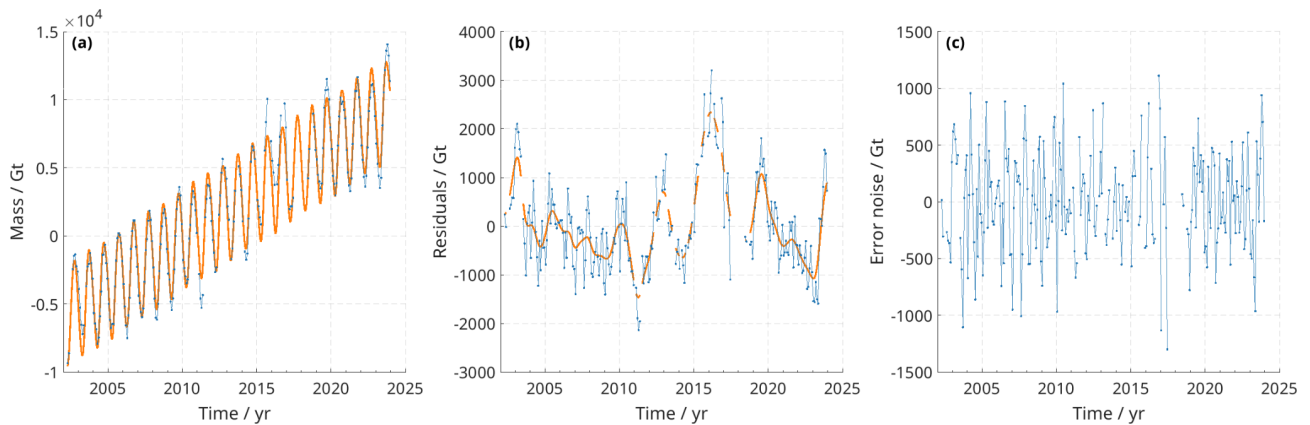
Figure 1 *Illustration of the process for quantifying the uncorrelated-noise component in the mass change time series of the global ocean. (a) Original mass change time series of the global ocean (blue) and the fitted model (orange). (b) Mass change residuals (blue) from subtracting the fitted model and after low-pass filtering (orange). (c) High-pass filtered residuals used for the assessment of the uncorrelated-noise based on the scaled standard deviation.*
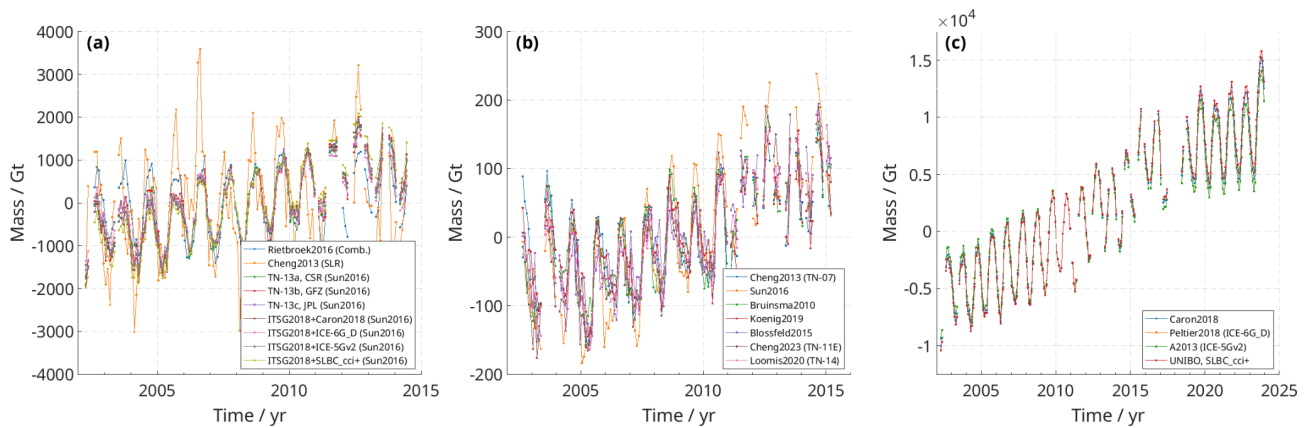
Figure 2 *Ensembles used for the assessment of errors propagated from the low-degrees and GIA. (a): degree-one contribution to global ocean mass change according to nine different sets of degree-one time series. (b): C_{20} contribution to global ocean mass change according to seven different sets of degree-one time series. (c): Global ocean mass change time series with four different GIA corrections.*

Error covariance matrices of each individual error source (Table 5) are summed up to the full error covariance matrix of the mass change time series. Figure 4 illustrates the covariance matrix for global ocean mass anomalies. Figure 4 b illustrates the uncertainties together with the time series of mass change of the global ocean (Figure 4 a). Note that the characterisation of temporally correlated errors of mass anomalies depends on the reference to which the anomalies refer. Here this reference is the mean mass distribution over the 11-year period 2005-01 - 2016-12.

Table 5 *Assessed uncertainty components for the ocean mass change integrated over the global ocean domain.*

Uncertainty component	Uncertainty on the global ocean domain
Temporally uncorrelated noise	**1.371 mm**
Trend uncertainty	
Trend uncertainty degree-one	0.170 mm yr^{-1}
Trend uncertainty C_{20}	0.011 mm yr^{-1}
Trend uncertainty GIA	0.175 mm yr^{-1}
Trend uncertainty leakage	0.099 mm yr^{-1}
Trend uncertainty combined	**0.264 mm yr^{-1}**
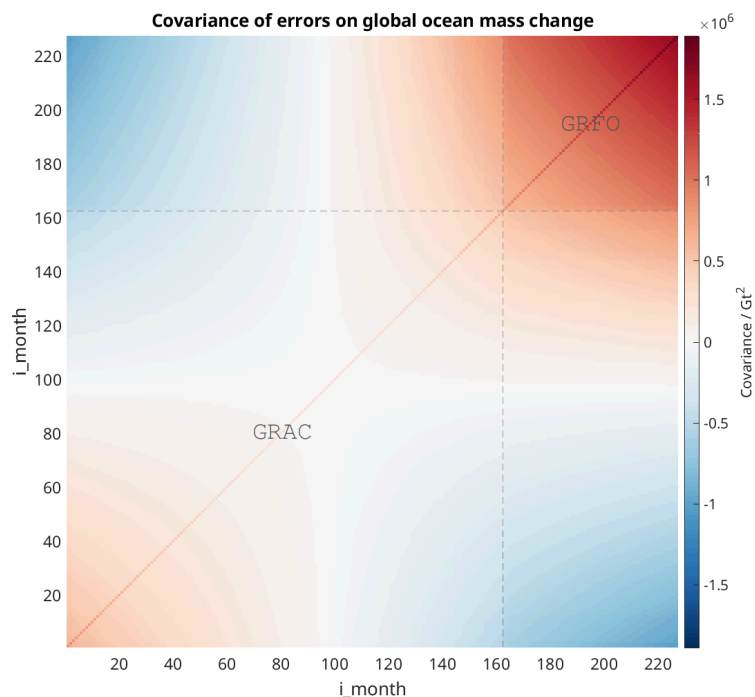
Figure 3 *Temporal error covariance matrix of the time series of global ocean mass anomalies corresponding to the TU Dresden L2-based mascon solution. The axis show sequential numbers of the monthly solutions, irrespective of temporal gaps (most notably the GRACE – GRACE-FO gap between No. 162 and 163).*

Figure 4 *(a) Global ocean mass changes (anomalies w.r.t. the mean over the reference period 2005-01 - 2016-12) and (b) their assessed uncertainties.*

3.4. Individual mass contributions

3.4.1. Land Water Storage component

The Land Water Storage component has been estimated using the Water Global Assessment and Prognosis (WaterGAP) Hydrological Model version 22e (Müller Schmied et al., 2024) (WGHM 22e). WGHM 22e provides estimates of LWS atmospheric reanalysis ERA5 and W5E5 datasets for the climat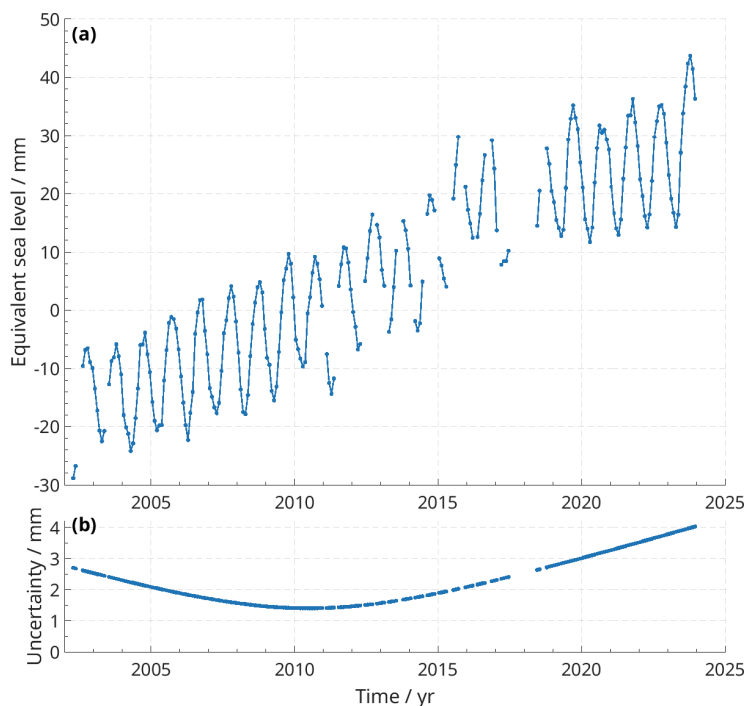e-forcing, with and without the anthropogenic contribution. The LWS time series used as a component for the sea level budget is obtained by averaging both WGHM 22e times series with the anthropogenic contribution.

Figure 5 shows the LWS time series used as a component for the sea level budget with its standard uncertainty. The uncertainty budget of the land water storage component includes two types of uncertainties:
- First, the uncertainty on the LWS trend, both for the climate-driven and anthropogenic contributions (Figure 7 green curve). We use the estimates obtained by Cáceres et al. (2020) over 1976-2002 (while the period does not perfectly coincide with our study period of 1993-2022, the time span is similar): -0.02 to 0.04 mm/yr for the climate-induced contribution and 0.14 to 0.25 mm/yr for the human-induced contribution. We use the range of these estimates as standard trend uncertainties, that is to say 0.06 mm/yr and 0.11 mm/yr for the climate-induced and human-induced contributions respectively.
- Second, we add white noise computed from the dispersion of the four WGHM solutions (ERA5 and W5E5 climate forcing and including or not the anthropogenic contribution, Figure 6a). Based on the difference of the ERA5 forced estimates, with and without anthropogenic contribution, the anthropogenic contribution is added to all time series that do not include the anthropogenic contribution (Figure 6b). The trend is removed from all time series (Figure 6c) as the trend uncertainty is already taken into account as described above. The standard deviation of the four curves from Figure 6c is used as uncertainty.

The combination of the two trend uncertainties and of the white noise results in a full covariance matrix of the LWS component, following the same methodology as for altimetry (Ablain et al., 2019; Guérou et al., 2023). The resulting standard uncertainty of the LWS time series is the orange curve on Figure 7. The period of reference used for the computation of uncertainties is 2005-2015 included. In other words, the uncertainty relates to the variations of LWS with respect to the average of LWS over 2005-2015.
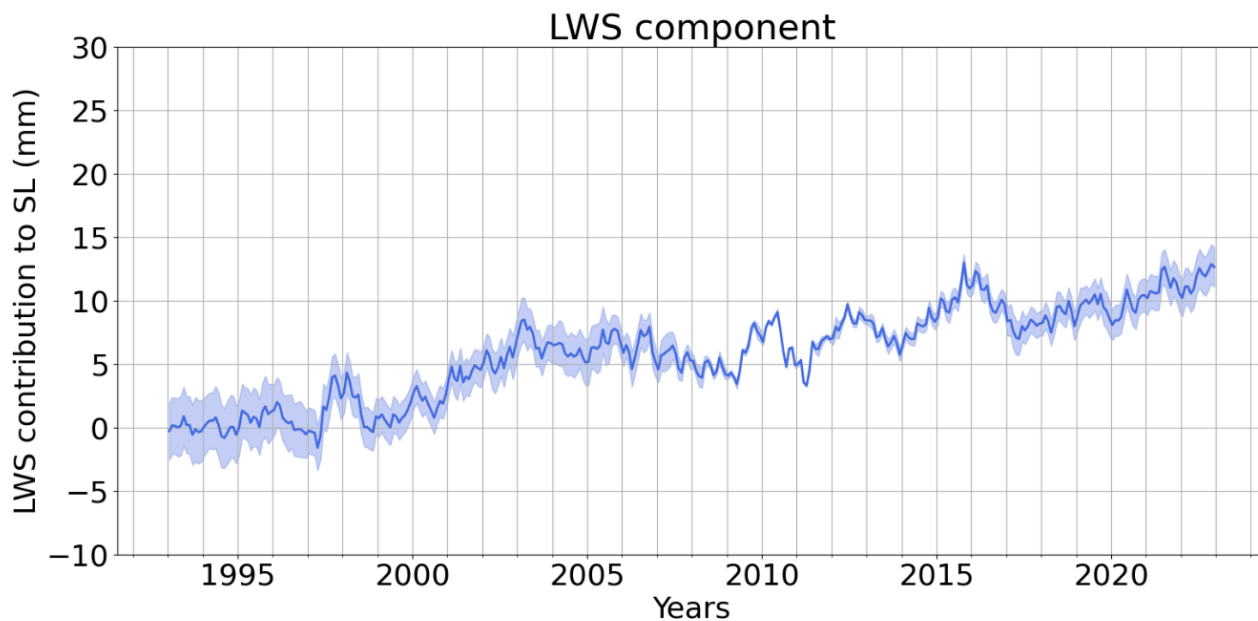
Figure 5 *Land water storage variations contribution to global mean sea level change obtained by averaging the WGHM 22e with ERA5 and W5e5 climate forcing and including the anthropogenic contribution with its standard uncertainty.*
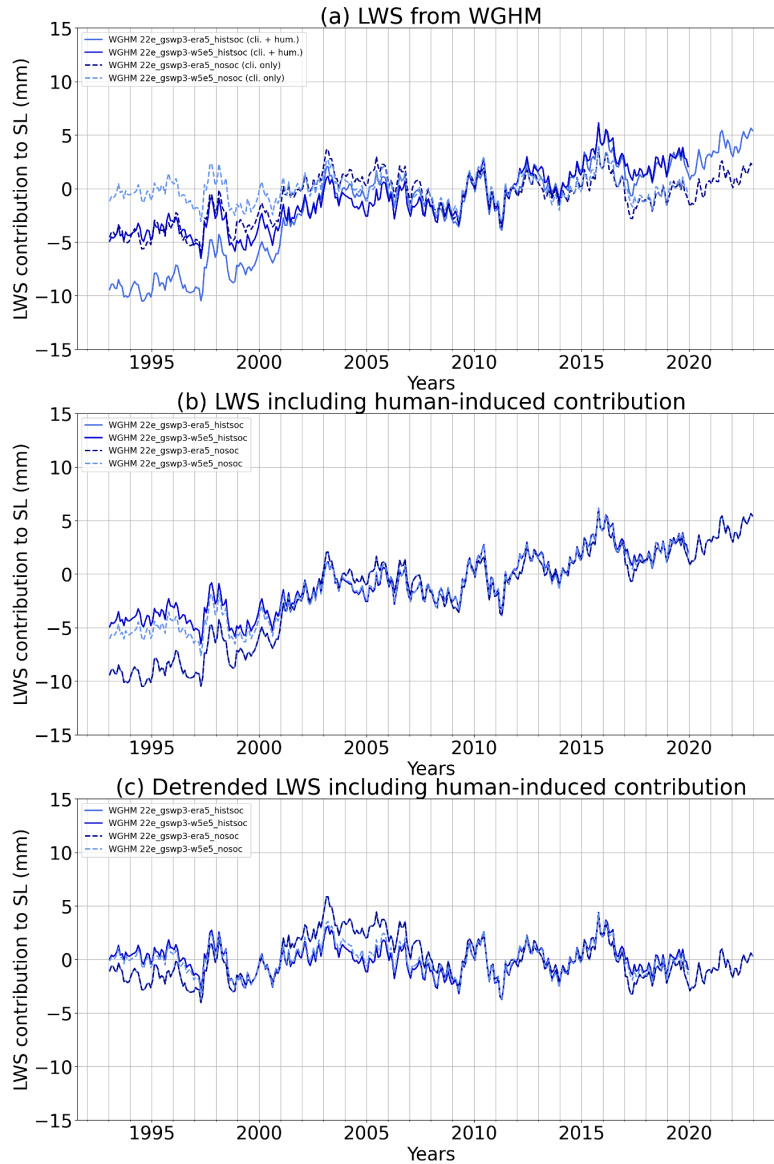
Figure 6 *Construction of ensemble of the estimate of the land water storage contribution uncertainty, using four WGHM 22e datasets. (a) WGHM 22e LWS contributions to global mean sea level with ERA5 and W5E5 climate forcing, with and without taking into account the anthropogenic contribution. (b) The anthropogenic contribution estimated from the differences between the two ERA5-forced time series is added to the time series without anthropogenic contribution. (c) Detrended time series.*
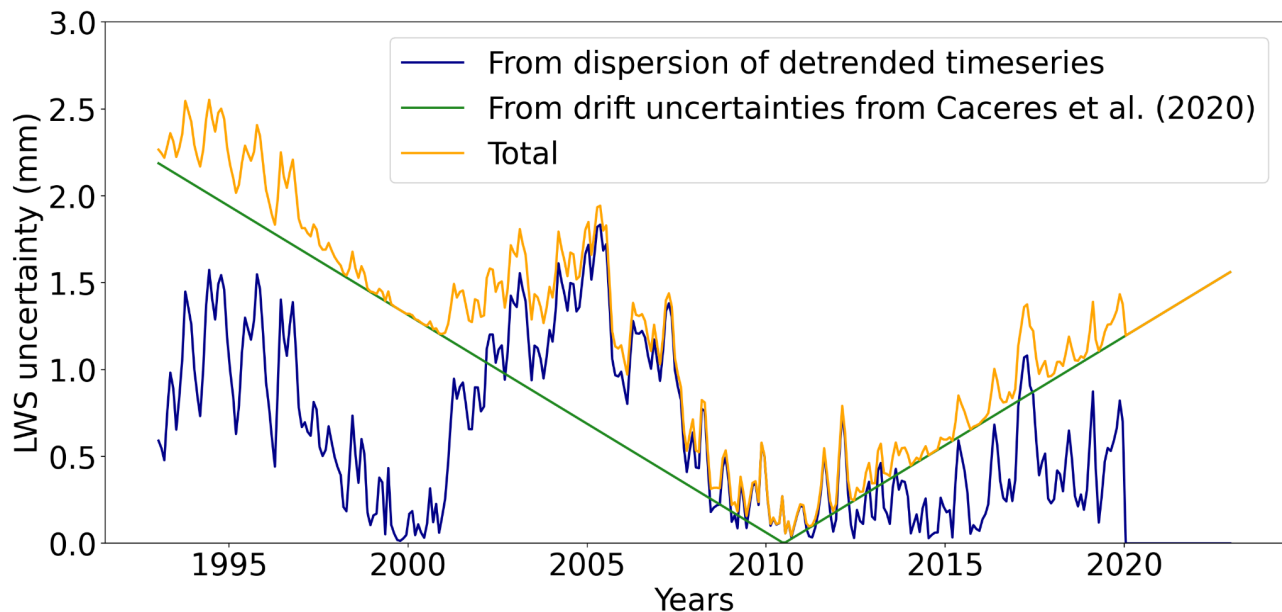
Figure 7 *Standard uncertainties of the land water storage contribution component. The blue curve results from the standard deviation of the ensemble of detrended estimates (see* Figure 5c). *The green curve accounts for the trend uncertainties for the climate-driven and human-induced contributions provided by Cáceres et al. (2020). The orange curve is the resulting combined standard uncertainty.*

It is important to highlight that we consider only one hydrological model providing estimates of LWS including the anthropogenic contribution and excluding the land ice contribution until the end of 2022. Besides, the uncertainties associated with the LWS component are likely to be underestimated. While we rely on the work of Cáceres et al. (2020) for the trend uncertainties, we only add white noise based on a few time series, not taking into account any time correlations.

3.4.2. Atmosphere water vapour component

The uncertainty on the Atmosphere water vapour component is estimated by computing the standard deviation of the different datasets available: ERA5 water vapour and combination of ESA CCI water vapour and Hambourg Ocean-Atmosphere Fluxes and Parameters from Satellite (HOAPS). More details about these 2 products are given in the PVIR ([AD1]). The common period of these 2 datasets is from 2002 to 2017.

This estimation of the standard deviation is propagated on the total time period of the ERA5 product (1993-2023) by modeling it as a pure white noise with a value 0.29 mm (at 1-sigma).

Figure 8 shows the Atmosphere water vapour component from ERA5 with its uncertainty over the period 1993-2023.
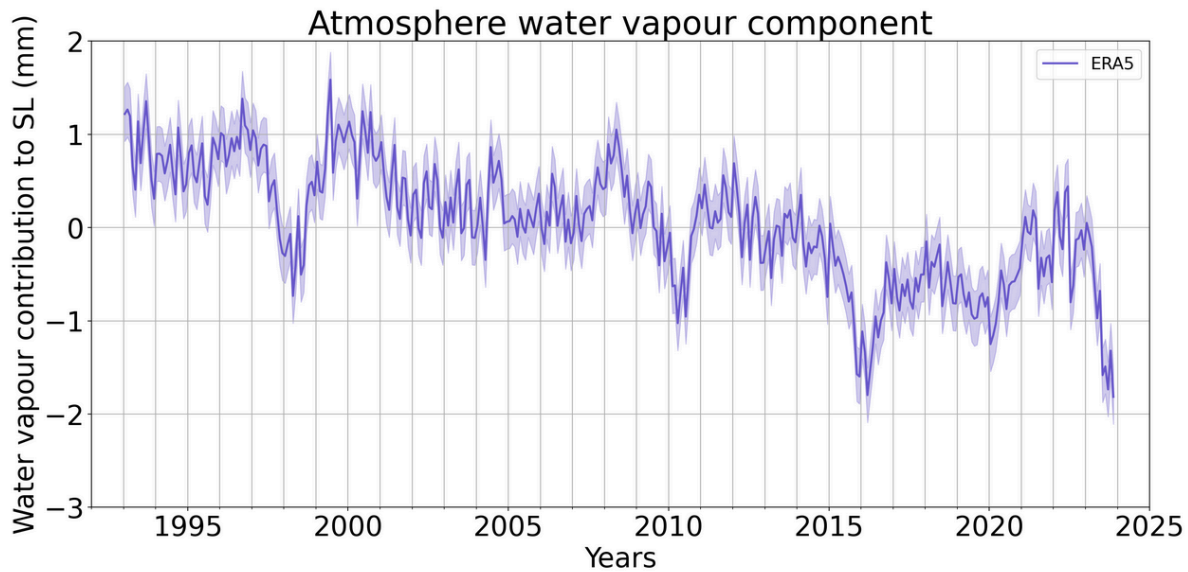
Figure 8 *Atmosphere vapour content from ERA over period 1993-2023*

3.4.3. Ice Sheets component

IMBIE-2_R2 aggregated assessment

Uncertainties from the contributed assessment are propagated through the IMBIE aggregation procedure by the formalism detailed by Otosaka et al. (2023). Since the cumulative mass balance is w.r.t. the start of the time series in 1992-01, given uncertainties of the cumulative mass balance are also w.r.t. this starting time and consequently increase monotonically in time. Uncertainties of cumulative mass anomalies w.r.t. a different reference time can be generated by cumulating the uncertainties of the mass balance rates w.r.t. the new reference time, adapting Eq. 7 of Otosaka et al. (2023).

For the AIS, Otosaka et al. (2023) quote an uncertainty at 18 Gt/a for the mean trend over 1992-2020. They quote larger uncertainties (between 39 Gt/y and 55 Gt/a) for each of the 5-year intervals considered within this overall assessment period. The relatively small uncertainty for the entire 1992-2020 interval arises from the assumption (implicit to Eq. 7 of Otosaka et al. 2023) that uncertainties of rates of mass change are uncorrelated from year to year.

For the GIS, Otosaka et al. (2023) quote an uncertainty at 16 Gt/a for the mean trend over 1992-2020. They quote larger uncertainties (between 29 Gt/y and 42 Gt/a) for each of the 5-year intervals considered within this overall assessment period.

CCI GMB products

Uncertainties of the monthly mass anomalies are modelled as the combined effect of uncertainties of the temporal linear trend, σ^2_{trend}, and a temporally uncorrelated noise, σ_{noise}. The uncertainties of linear trends are summed up in quadrature from uncertainties due to different error sources (b, c, d

outlined in Section 2.3.4). The trend uncertainties are given separately. In this way, it can be propagated to monthly uncertainties w.r.t. a reference time of the user's choice. The error variance at any epoch is then $\sigma^2_{total}(t) = \sigma^2_{noise} + \sigma^2_{trend} (t - t_0)^2$.

For the AIS, the CCI GMB (cf. DARD Table 23, now updated to Release 5.0) quotes $\sigma_{trend} = 44$ Gt/a, $\sigma_{noise} = 88$ Gt. For the GIS, the CCI GMB (cf. DARD Table 19, now updated to Release 4.1) quotes $\sigma_{trend} = 14$ Gt/a, $\sigma_{noise} = 44$ Gt. The values for σ_{trend} are applicable as uncertainties of long-term trends over any multi-year periods because most of the error sources for multi-year trends are systematic errors on the trends and do not significantly average out when the time period gets longer.

3.4.4. Glaciers component

The uncertainty in the GIC component was generated by the data providers (WGMZ, Univ Zurich) and the methodology is described in detail in the paper associated with the product Dussaillant et al. (2024). In summary, it uses a leave one out cross validation approach for each GIC region and the values provided are 2 sigma. There are, however, some important differences in the magnitude of the uncertainty before and after the year 2000. The approach taken uses *in-situ* mass balance data for individual glaciers to calibrate geodetic mass balance estimates from DEM differencing (Hugonnet et al., 2021) derived primarily from ASTER imagery. These data have high spatial fidelity but low temporal fidelity. Typically they can only provide reliable decadal trends at glacier level and the time series is from 2000-2020. Prior to 2000, the uncertainties are consequently about a factor three larger when integrated globally (Figure 9).
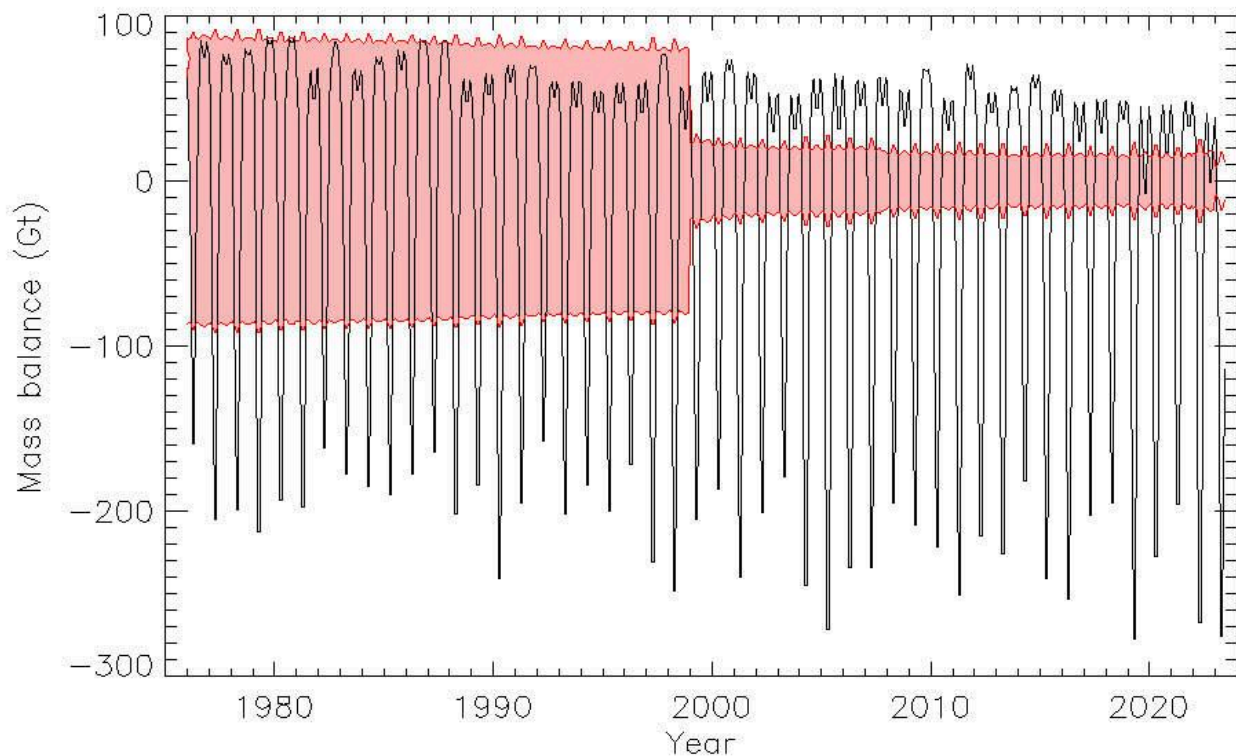
Figure 9 *Monthly resolved GIC mass balance from 1976–2023 inclusive in black. 2-sigma uncertainties in shaded red.*

Note, that the 0.5 deg resolution grid cells have been summed to produce both mass balance and uncertainty making the assumption that spatial errors are correlated but while those in time are uncorrelated. Due to the methodology used to construct the time series, uncertainties scale inversely with the number of *in-situ* observations and are largely in regions with few observations (Dussaillant et al, 2024). For the period after year 2000, the spatially aggregated 2-sigma uncertainties are less than ±0.1 mm/yr SLE. Prior to this it is close to ±0.3 mm/yr SLE.

3.5. Glacial Isostatic Adjustment and Present Days Ice Melting component

Modelled GIA (glacial isostatic adjustment) and PDIM (the present day ice melting component) of present sea level are affected by uncertainty stemming from various sources. In consequence of that, the data available from *https://doi.org/10.5281/zenodo.12755218* (Spada and Melini, 2019) are characterized by some relevant uncertainties, and in particular:

- For elastic fingerprints, the uncertainties arise from i) the finite discretization scheme adopted for the Sea Level Equation, ii) the assumption of a specific 1D structure of the elastic Earth model. From a suite of tests, we have quantified these uncertainties as +/- 5% relative error on all the elastic fingerprints evaluated for a specific (uncertainty-free) time history of the surface load.

- For GIA, given a spherically symmetric rheological model, uncertainties arise because of our imperfect knowledge about the viscosity profile with increasing depth in the mantle. To quantify this uncertainty, we have considered ICE-6G_C ensemble standard deviations (1-sigma) over the 20 variations of the "VM5a" rheological profile defined in section 5 of the work of Roy and Peltier (2015). The nominal ICE-6G-C model has been introduced by Argus et al. (2014) and Peltier et al. (2015).

Known intrinsic limitations of the GIA and PDIM modeling reside upon the assumed 1-D (i.e., spherically symmetric) viscoelastic structure of the model adopted.

4. Analysis of the unconstrained SLBC: Historical Approach

This section presents the results obtained using the classical "historical" approach for the sea level budget (SLB) following the methodology described in the PVIR [AD1] and ATDB [AD3].

We first analyse the ocean mass and sea level budget at the global mean scale, then extend the analysis to the regional scale. All estimates include an uncertainty characterization derived from the propagated uncertainties on each budget component.

The goal is to provide a full characterization of uncertainties affecting the SLB results, and to assess their impact on the reliability of the conclusions derived from the budget analysis.

4.1. At global mean

4.1.1. Mass budget

The global mean ocean mass budget is computed using the following relation:

$$S = (\Delta GMSL_{bary})_{sat} - \big[(\Delta GMSL_{bary})_{GIS} + (\Delta GMSL_{bary})_{AIS}$$

$$+ (\Delta GMSL_{bary})_{GIC} + (\Delta GMSL_{bary})_{LWS} + (\Delta GMSL_{bary})_{WV}\big]$$

Equation 1

Where :

- $(\Delta GMSL_{bary})_{sat}$ is the ocean mass change estimated from GRACE/GRACE-FO data.
- The sum:
  $[(\Delta GMSL_{bary})_{GIS} + (\Delta GMSL_{bary})_{AIS} + (\Delta GMSL_{bary})_{GIC} + (\Delta GMSL_{bary})_{LWS} + (\Delta GMSL_{bary})_{WV}]$
  represents the cumulative mass input from individual components (Greenland ice sheet, Antarctic ice sheet, glaciers and ice caps, land water storage, and atmospheric water vapour).

The mass budget residual, S, indicates the degree of closure between the mass observed by gravimetry and the sum of individual sources.

The associated uncertainty is obtained by error propagation:

$$\sigma_S^2 = \sigma_{(\Delta GMSL_{bary})_{sat}}^2 + \sigma_{(\Delta GMSL_{bary})_{GIS}}^2 + \sigma_{(\Delta GMSL_{bary})_{AIS}}^2$$

$$+ \sigma_{(\Delta GMSL_{bary})_{GIC}}^2 + \sigma_{(\Delta GMSL_{bary})_{LWS}}^2 + \sigma_{(\Delta GMSL_{bary})_{WV}}^2$$

Equation 2

Where all terms are assumed independent.

The Figure 10 presents the global mean barystatic sea level time series over the GRACE/GRACE-FO period with the corresponding uncertainties. Panel (a) shows the total barystatic sea level rise estimated directly from GRACE/GRACE-FO data (solid blue line) and from the sum of individual mass components (dashed blue line). The contributions of the major sources are also plotted: glaciers in purple, Greenland ice sheet in green, Antarctic ice sheet in yellow, and land water storage in teal. We note that the uncertainty associated with the GRACE-based barystatic estimate is generally smaller than that derived from the sum of individual mass components. This difference largely stems from the relatively large uncertainties in the mass loss estimates from the ice sheets (Antarctica and Greenland). Overall, the agreement between the two

barystatic sea level estimates is good throughout most of the common period. As shown in panel (b), the difference between the GRACE-based and reconstructed barystatic sea level remains within the uncertainty bounds in the majority of the time series, suggesting a satisfactory closure of the global mean ocean mass budget within the current uncertainty range.

Nevertheless, two specific periods stand out where the discrepancy exceeds the uncertainty envelope: from 2015 to mid-2017, and from 2019 to 2020. These time intervals coincide with significant climate anomalies, the strong El Niño event of 2015–2016 and the La Niña event of 2019–2020. Such large-scale climate fluctuations are known to drive strong interannual variability in precipitation patterns and continental water storage, which may not be fully captured by the land water storage estimates derived from reanalysis-based models. This likely contributes to the observed mismatch during these periods.
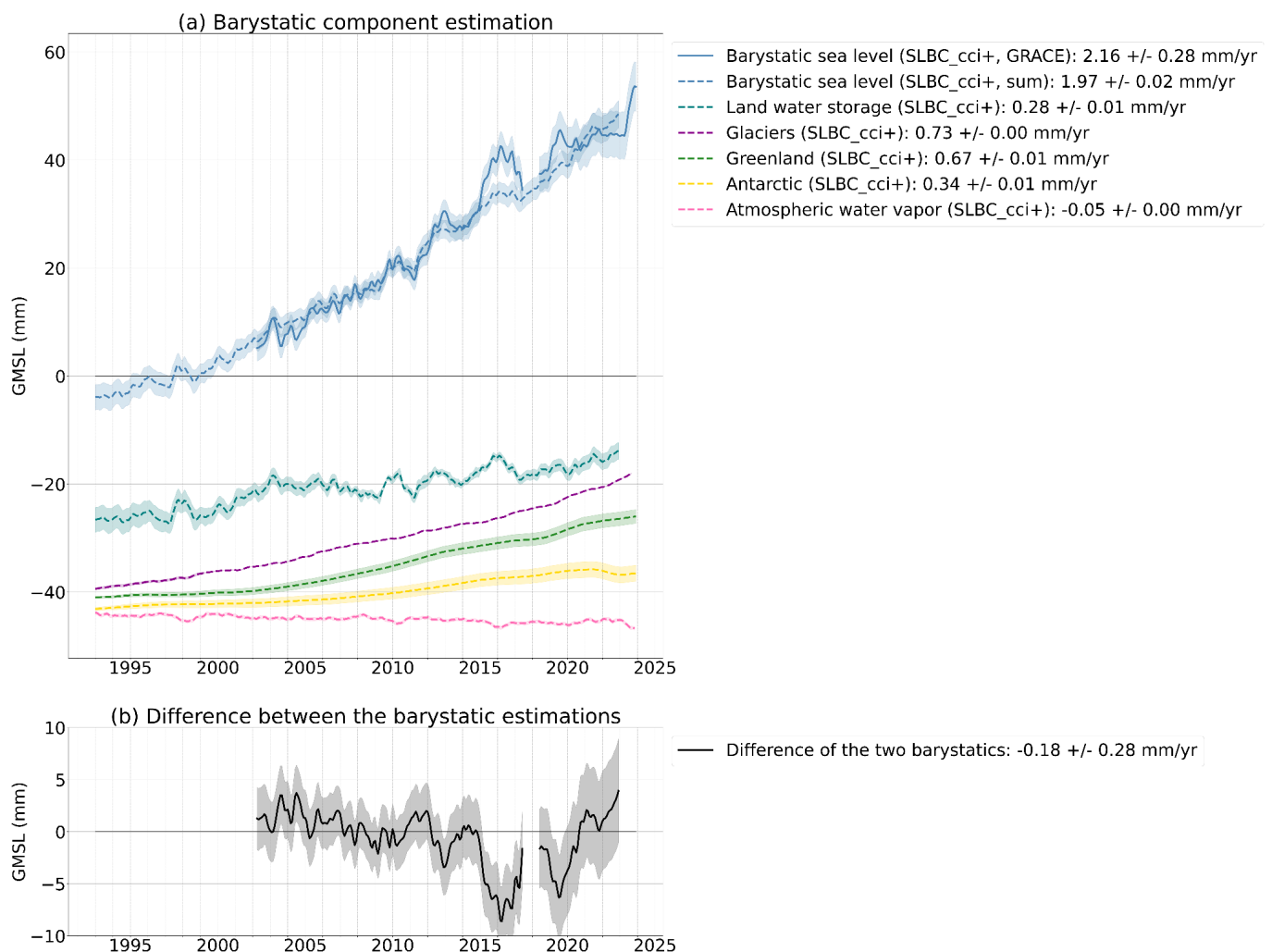
Figure 10 *(a) Global mean barystatic sea level time series for SLBC CCI+. Blue lines show the total barystatic component: solid for barystatic from GRACE/GRACE-FO data, and dashed for barystatic from the sum of individual mass components. Teal lines show land water storage, purple lines show glacier melt, green lines Greenland Ice Sheet mass loss, and yellow lines Antarctic Ice Sheet mass loss. (b) Difference between barystatic sea level estimates from GRACE/GRACE-FO*

and sum of individual mass components. Uncertainty envelopes are displayed around each time series using the corresponding color, representing the 1-sigma uncertainty for each time series. Trends estimated over the period 06/2002 - 12/2022.

4.1.2. Sea level budget

The global mean sea level budget is computed as:

$$R = (\Delta GMSL_{rel})_{alti} - [(\Delta GMSL_{bary})_{gravi} + (\Delta GMSL_{steric})_{in\ situ}]$$ Equation 3

Where:

- $(\Delta GMSL_{rel})_{alti}$ is the relative sea level change measured by satellite altimetry and corrected for global mean vertical land motions related to GIA and present day ice melting, or the changes in the height of the seafloor relative to the reference ellipsoid.
- $(\Delta GMSL_{bary})_{gravi}$ is the ocean mass change from gravimetry (GRACE/GRACE-FO) corrected for GIA.
- $(\Delta GMSL_{steric})_{in\ situ}$ is the steric sea level change derived from in-situ temperature profiles.

The uncertainty on the budget residual is:

$$\sigma_R^2 = \sigma_{(\Delta GMSL_{rel})_{alti}}^2 + \sigma_{(\Delta GMSL_{bary})_{gravi}}^2 + \sigma_{(\Delta GMSL_{steric})_{in\ situ}}^2$$ Equation 4

The uncertainty analysis for the sea level budget is currently limited to the 2005–2020 period, as uncertainties on the steric component at global scale are only available over that time range in the present version of the dataset. This will be extended to the full time span in a future version of the document. Within this constrained period, Figure 11b reveals distinct patterns in budget closure depending on the barystatic estimate used. When the ocean mass contribution is taken from the sum of individual mass components, the sea level budget residuals is significant and exceeds the uncertainty bounds during 2005–2007, as well as from 2015 onwards. Between 2007 and 2015, the SLB is closed within uncertainties using the individual mass contributions approach, suggesting a good estimation of the ocean mass variations during that interval.

In contrast, when GRACE/GRACE-FO data are used directly for the barystatic component, the budget shows much better closure, with residuals remaining within uncertainty bounds from 2005 through mid-2017. After this point, however, the residuals become significant again, indicating a mismatch between observed and reconstructed sea level that cannot be explained by the stated uncertainties. This discrepancy may result from several possible causes, including underestimated uncertainties, inconsistencies between observational systems, the presence of biases or drifts in one or more datasets, or even a missing contribution in the budget formulation.

It is also worth noting that, among all components, the steric contribution carries the largest uncertainties throughout the analysed period. While this does not necessarily explain the observed residuals, it highlights the importance of improving the accuracy and uncertainty quantification of thermosteric measurements in order to better constrain the sea level budget. Moreover, the observed differences between the two barystatic estimates call for further investigation (particularly

on the side of the mass component summation). A more detailed analysis of the internal consistency between the individual mass contributions (e.g., ice sheets, glaciers with or without peripheral glaciers, land water storage) is needed to assess whether discrepancies in their aggregation could be contributing to the mismatch with GRACE-based estimates and the associated budget closure issues.
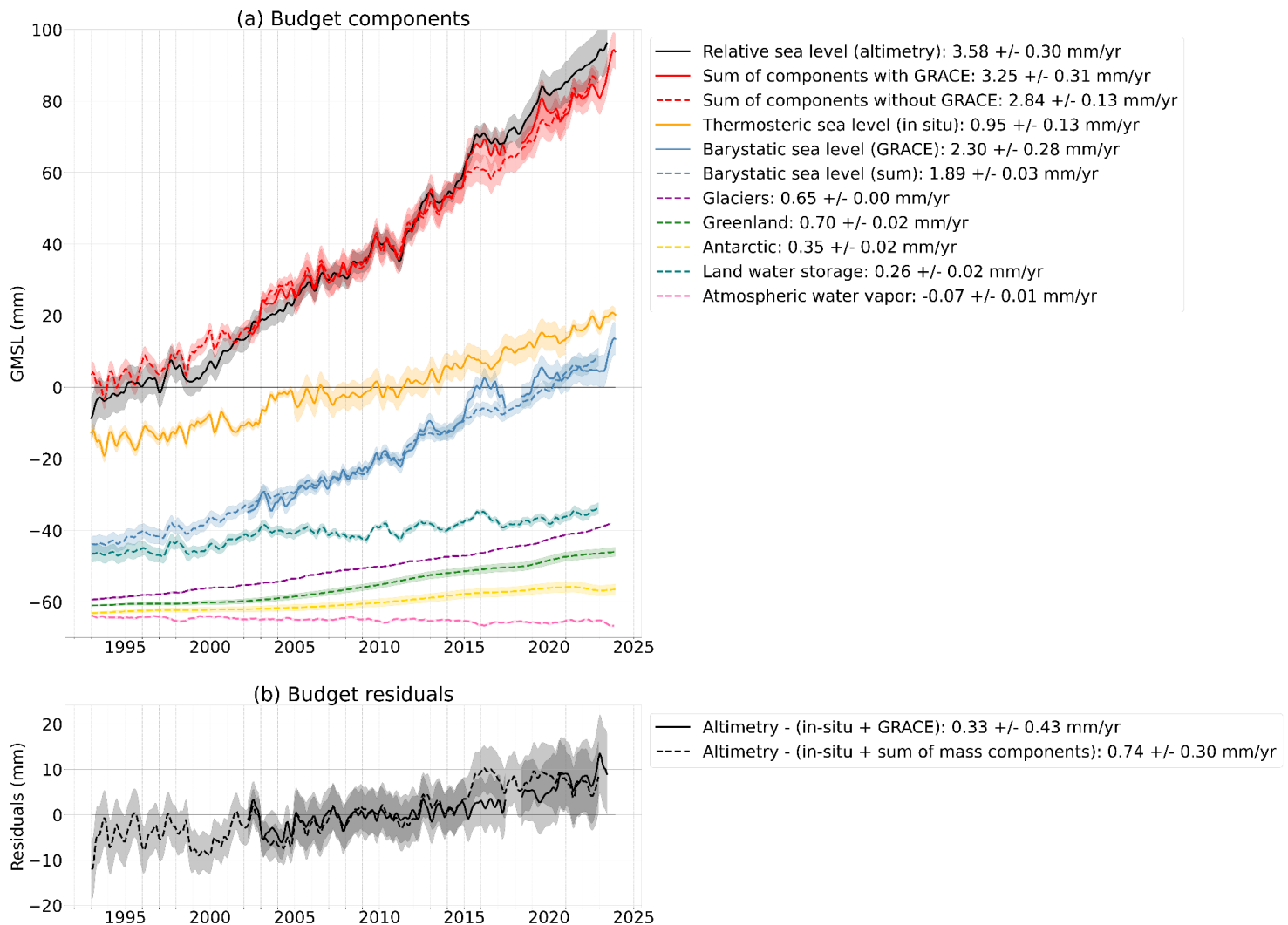
Figure 11 *Sea level budget comparison using two different barystatic components. (a) Global mean sea level budget components using SLBC CCI+ data. The black curves represent altimetry-based sea level; the blue curves show the manometric (barystatic) component from GRACE; the orange curve shows the thermosteric contribution, respectively; and the red curves show the sum of all components. Solid lines indicate values based on GRACE-derived barystatic sea level; dashed lines indicate values based on the sum of individual mass contributions. (b) Residuals of the sea level budget, computed as the difference between the observed sea level (altimetry) and the sum of all components. Uncertainty envelopes are displayed around each time series using the*

corresponding color, representing the 1-sigma uncertainty for each time series. Trends estimated over the period 06/2002-06/2016.

4.2. At regional scale

At the regional scale, the sea level budget is assessed for each local point as:

$$r = (\Delta SL_{rel})_{alti} - [(\Delta SL_{man_{GIA}})_{gravi} + (\Delta SL_{steric})_{in~situ}] \qquad \text{Equation 5}$$

Where:

- $(\Delta SL_{rel})_{alti}$ is the relative sea level change measured by satellite altimetry and corrected for the vertical land motions related to GIA and current days ice melting, or the changes in the height of the seafloor relative to the reference ellipsoid.
- $(\Delta SL_{man_{GIA}})_{gravi}$ is the manometric sea level change from gravimetry (GRACE/GRACE-FO) corrected for GIA.
- $(\Delta SL_{steric})_{in~situ}$ is the steric sea level change derived from in-situ temperature profiles.

The uncertainty on the residuals is simply the sum of the uncertainties of each component involved in the budget:

$$\sigma_r^2 = \sigma_{(\Delta SL_{rel})_{alti}}^2 + \sigma_{(\Delta SL_{man_{GIA}})_{gravi}}^2 + \sigma_{(\Delta SL_{steric})_{in~situ}}^2 \qquad \text{Equation 6}$$

Figure 12 presents the spatial distribution of sea level trends from April 2002 to December 2019 based on observed altimetry (panel a), the main budget components : GRACE-based manometric (panel b), Argo-based thermosteric (panel c), and halosteric (panel d) sea level; and the residuals of the budget (panel e), computed as the difference between the observed sea level and the sum of components. Hatched areas indicate where the trend is not statistically significant compared to the associated uncertainties, while non-hatched regions correspond to significant trends.

Overall, most of the trends derived from satellite altimetry (a) and the GRACE-based barystatic (b) component are significant. In contrast, the thermosteric (c) and halosteric (d) trend maps exhibit larger hatched areas, highlighting that many of their regional signals are not statistically distinguishable from noise. This reflects the larger local uncertainties associated with these components.

These uncertainties were estimated from the spread between two monthly steric datasets: the ISAS20 product used in this project and the EN4 T/S database version 2.2 (Good et al., 2013). For each grid cell, trend uncertainties were derived from the dispersion between the products with respect to their mean. For total steric sea level, thermosteric, and halosteric contributions, the uncertainties were quadratically combined. In future versions of this analysis, these uncertainties will be refined using a full error budget approach rather than relying on inter-product spread.

Figure 13 shows the anomaly maps of sea level trends over the same period shows the trend anomaly map, where the global mean trend has been subtracted to highlight regional deviations.

As with the absolute trends, most significant features in the altimetry and GRACE-derived fields are retained, whereas larger portions of the steric fields remain statistically insignificant. The residual trend maps from both figures allow us to assess where the sea level budget is locally closed. Areas with hatched patterns in panel (e) indicate regions where the residual trend is within the range of uncertainties, suggesting local closure of the budget.

Using the SLBC CCI+ dataset components, several notable regions of non-closure emerge. Strong positive residual trends are observed near coastlines, large spatial scale regions of non-closure appear especially around South America, and in the southern Indian Ocean. These may be related to limitations in the representation of near-coastal processes or unaccounted-for contributions. Significant residuals are also seen in high-resolution features captured by altimetry but unresolved by GRACE, such as in the Antarctic Circumpolar Current region. Furthermore, the GRACE data used here have not yet been corrected for known coseismic displacements related to the Sumatra (2004), Maule (2010), and Tohoku-Oki (2011) earthquakes, and these signals are clearly visible in the residual trend maps. In the North Pacific, budget residuals trace the paths of the Kuroshio and North Equatorial Currents, which are strongly observed in altimetry but not in the gravimetric data, again likely due to differences in spatial resolution between observing systems.

In conclusion, under the current state of uncertainty estimation, the residuals observed in regions where the sea level budget does not close cannot be fully explained by the provided uncertainty envelopes. One promising avenue for improving the interpretation of these residuals lies in assessing the impact of observability errors (see Section 5), particularly those arising from differences in spatial resolution and observational configurations across measurement systems. This is especially evident in the discrepancies between altimetry and gravimetry, where high-resolution oceanic features detected by altimetry remain largely unresolved by GRACE, pointing to potential mismatches in the phenomena each system is capable of capturing.
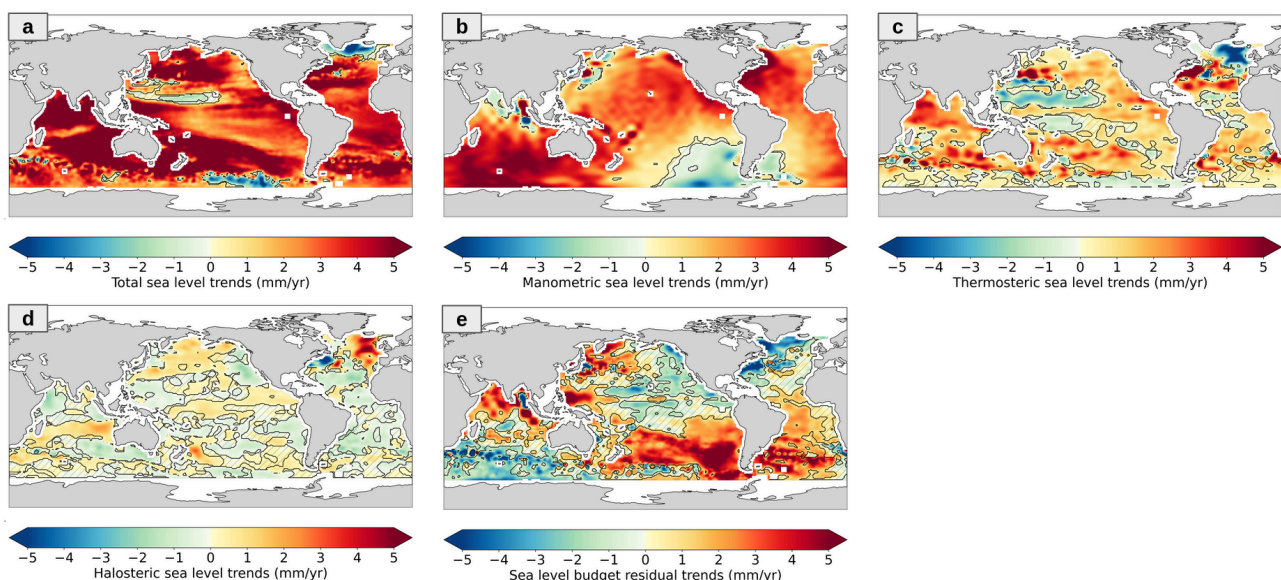

Figure 12 *Sea level trends over April 2002 to December 2019 in observed altimetry-based sea level (a), components (b, c, d: GRACE-based manometric, Argo-based thermosteric and Argo-based halosteric sea level) and budget residual trends (observed sea level minus sum of*

components) (e). Hatched areas indicate regions where the trend is not statistically significant compared to the associated uncertainties; non-hatched areas correspond to significant trends.
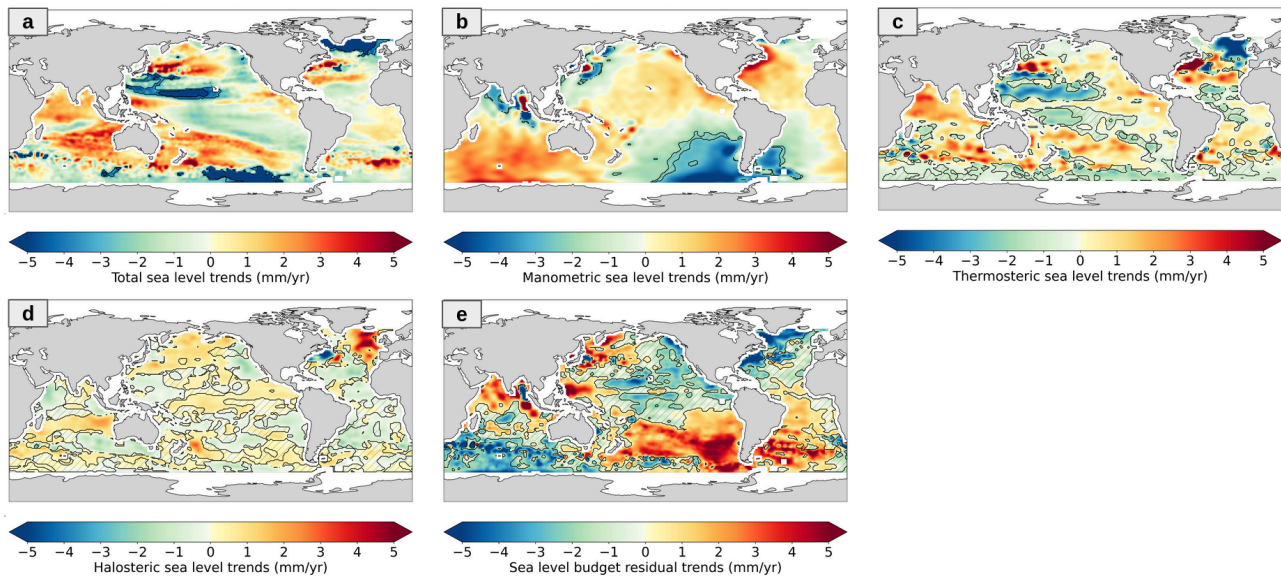

Figure 13 *Sea level trends anomalies over April 2002 to December 2019 in observed altimetry-based sea level (a), components (b, c, d: GRACE-based manometric, Argo-based thermosteric and Argo-based halosteric sea level) and budget residual trends (observed sea level minus sum of components) (e). Hatched areas indicate regions where the trend is not statistically significant compared to the associated uncertainties; non-hatched areas correspond to significant trends.*

5. Analysis of the objectively constrained SLBC: Innovative Approach

As detailed in the project proposal ([AD6]), the objective of this approach aims to deliver an objective solution to the Sea Level Budget (SLB) by optimally combining sea level components in a way that minimizes the budget residuals within the uncertainty bounds of each component. The project proposal [AD6] details the goal of this approach, which is to find an objective solution to the Sea Level Budget (SLB). This will be achieved by optimally combining sea level components to minimize budget residuals, all while staying within the uncertainty bounds of each component. This objective method will enable us to pinpoint dates and places where the SLB does not close within uncertainties along with the contribution that is most probably responsible for the misclosure.

To perform a rigorous objective method, the description of the uncertainties of the Sea Level Budget (SLB) components is a key point that needs to be done. During this project, the objective was to decompose the uncertainties into 2 different sources:

1) The structural uncertainty of the SLB associated to the effective resolution of the current observing system,

2) And the measurement uncertainties of the SLB associated with the instrumental error and the algorithmic approximations of each observing system that measures an individual contribution to sea level.

Measurement uncertainties are the one that have been estimated for each component and described in section 3.

Structural uncertainty represents the level of uncertainty in the SLB that would remain even if sea level and its individual components were measured perfectly. It reflects residual inconsistencies arising from mismatches in the spatial and temporal resolution across the various observing subsystems—for example, differences in resolution between Argo, GRACE, and satellite altimetry. This type of uncertainty offers a quantitative measure of how well the SLB can be observed using the current observing system and sets a lower bound on the system's uncertainty.

The estimation of these uncertainties has been made by using synthetic observations for altimetry, gravimetry and in-situ observing systems from a numerical ocean-sea-ice simulation produced as part of the OCCIPUT project (Bessières et al., 2017). This model provides outputs of several members at a 5-day frequency for 3-d (x,y,z) variables (such as temperature, salinity, velocities, etc) and at daily frequency for 2-d (x,y) variables (such as Sea Surface Height SSH, Sea Surface Temperature SST, bottom pressure, sea-ice properties, etc).

Along with these gridded model outputs, some "synthetic" observations have also been extracted from each member at the times and locations of true observations included in the following datasets:

- the EN4 collection of individual Temperature and Salinity profiles (which includes Argo, CTDs, XBT, TAO, etc ; see Good et al., 2013),
- the along-track altimetry database from the TOPEX, Jason-1, Jason-2 and Jason-3 satellite series.

A precise detail of the processing applied on these synthetic data is provided in section 2.10 of the ATBD ([AD3]) as well as a diagram in Figure 14.
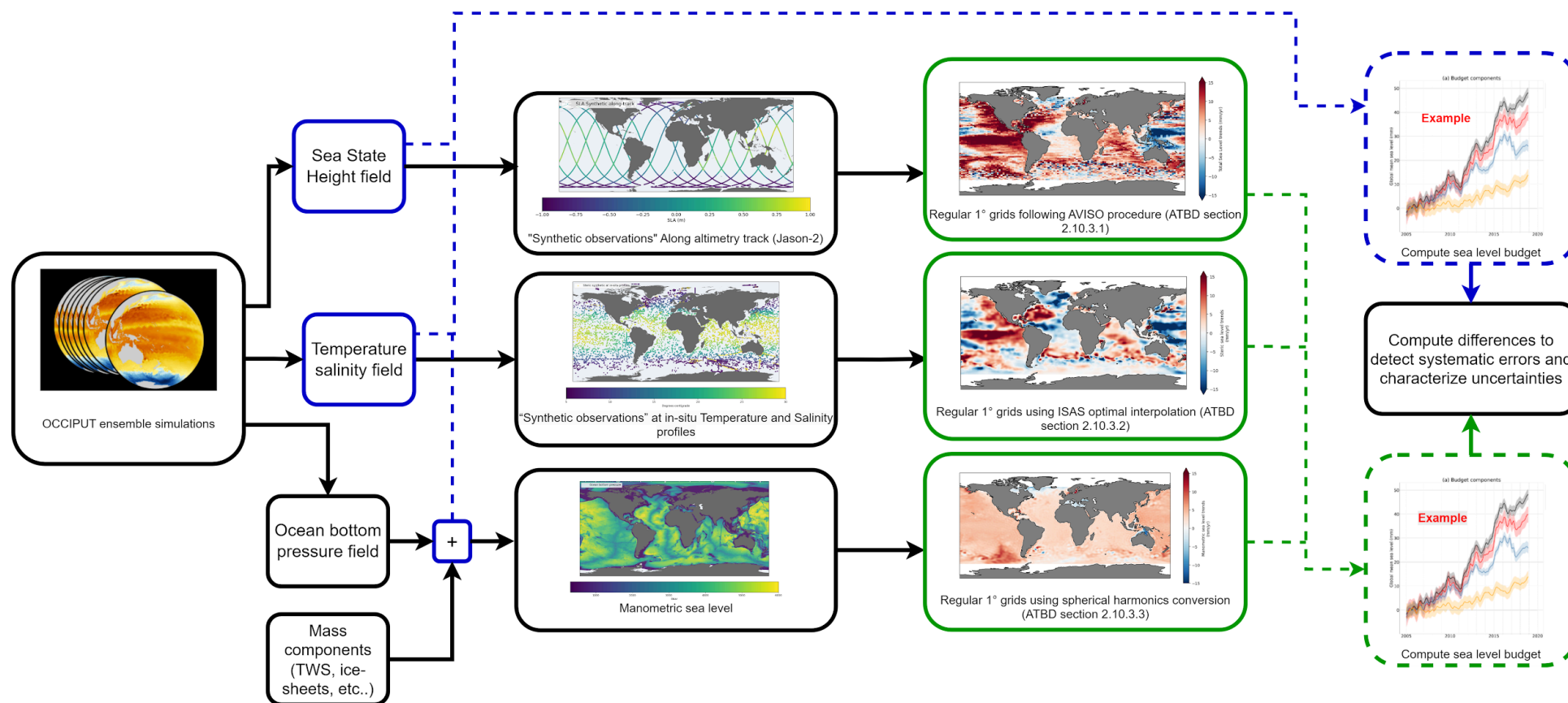
Figure 14 *diagram describing the processing of synthetic data to derive structural uncertainties of each SLB component*

5.1. At global mean

To assess how observational systems (altimetry, gravimetry, in situ profiles) contribute to observability uncertainties in each component, the SLB component from the OCCIPUT ocean model (blue boxes in Figure 14) will be compared to the reconstructed component from its corresponding observing system (green boxes in Figure 14). These comparisons will be performed at global scale over the period of availability of the model 2009-2015.

Figure 15 shows the evolution of the difference between the relative sea level from the OCCIPUT ocean model minus the relative sea level reconstructed with synthetic observations following the procedure detailed section 2.10.3.1 of the ATBD. We can observe over the period 2009-2015 a positive linear trend of 0.20 mm/yr.

Figure 15 *Relative sea level from OCCIPUT ocean model minus relative sea level at observation location (dashed line) and with 1-year filter (solid line) over period 2009-2015*

Figure 16 shows the evolution of the difference between the thermosteric sea level from the OCCIPUT ocean model minus the thermosteric sea level reconstructed with synthetic observations following the procedure detailed section 2.10.3.2 of the ATBD. We can observe over the period 2009-2015 a negative linear trend of -0.26 mm/yr.
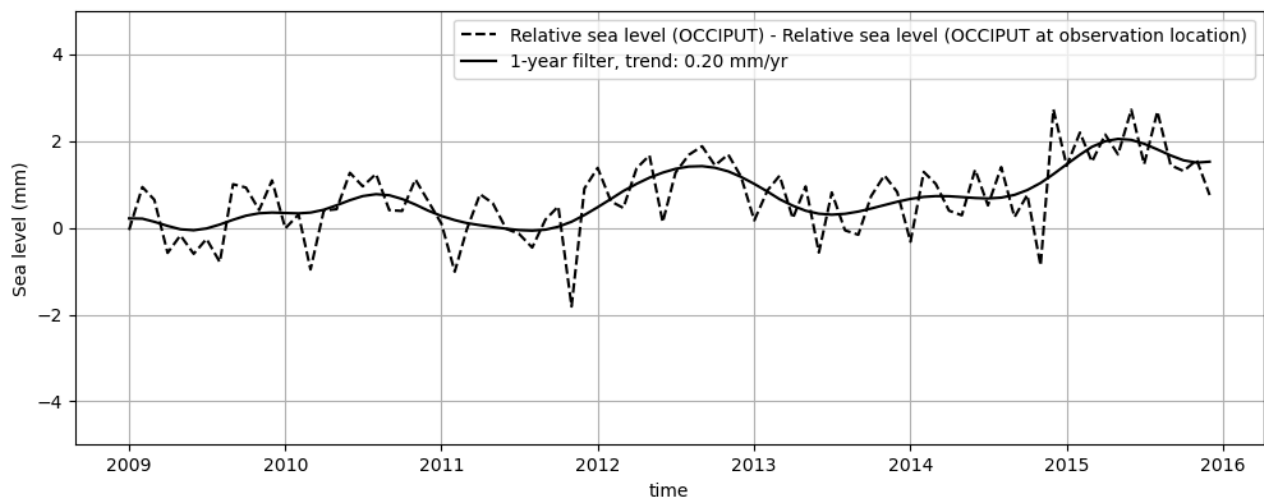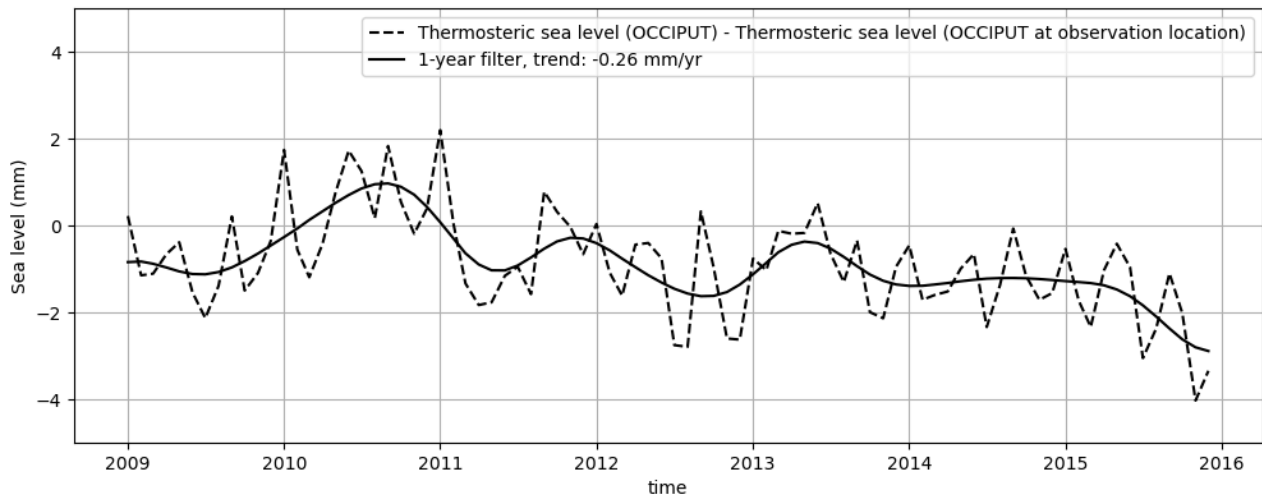
Figure 16 *Steric sea level from OCCIPUT ocean model minus steric sea level at observation location (dashed line) and with 1-year filter (solid line) over period 2009-2015*

Figure 17 shows the evolution of the difference between the barystatic sea level from the OCCIPUT ocean model minus the barystatic sea level reconstructed with synthetic observations following the procedure detailed section 2.10.3.3 of the ATBD. We can observe over the period 2009-2015 a very weak negative trend of -0.03 mm/yr.
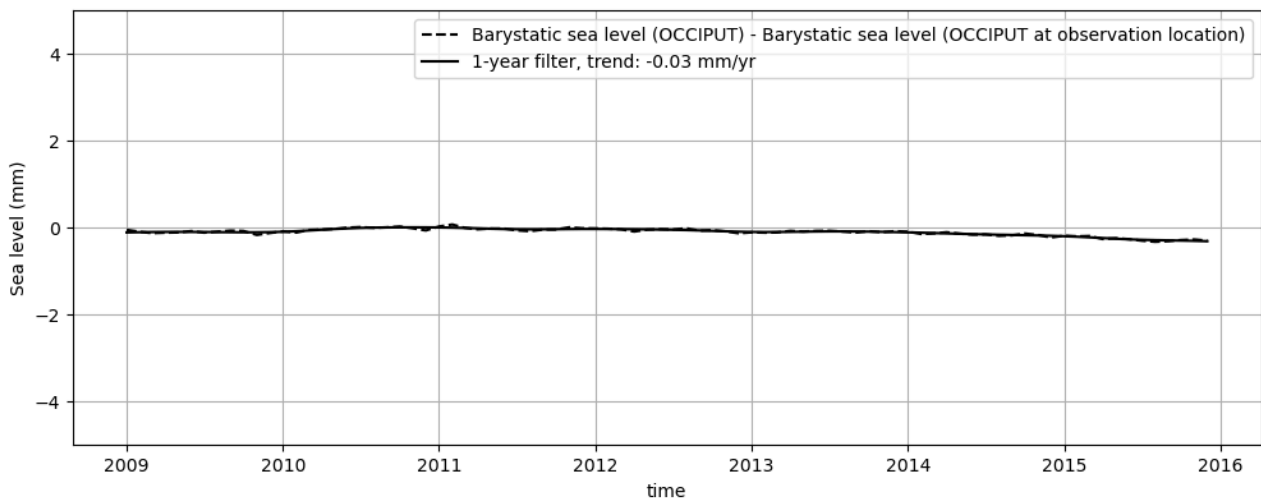
Figure 17 *Barystatic sea level from OCCIPUT ocean model minus barystatic sea level at observation location (dashed line) and with 1-year filter (solid line) over period 2009-2015*

Figure 18 shows the variances of the different components of the SLB estimated with the synthetic data at yearly timescale. As seen in previous figures, we can observe that the variances on the relative and steric sea level are much larger (respectively 0.4 mm² and 0.6 mm²) compared to the barystatic sea level. Also we can observe on the relative sea level measured by altimetry a periodic signal of 3 years with larger variances that should be investigated.

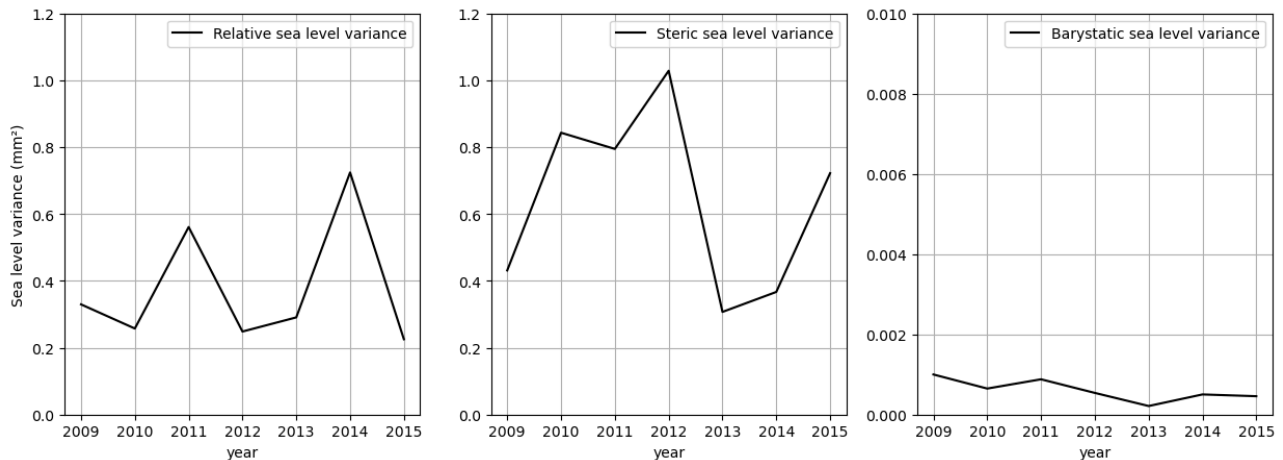Figure 18 *Sea level variance at 1 year of relative sea level (left), steric sea level (middle) and barystatic sea level (right) of the component at observation location evolution over the period 2009-2015*

Even if the synthetic data provided are not totally representative of the reality (e.g. only one altimetry along-track mission is provided while several missions are used for L4 products provided such as C3S dataset), it can be used to provide a first estimation of the observability uncertainty that could be refined in the future.

The estimation of the variances of each synthetic component enables to provide an estimation of the observability uncertainty due to their respective observing system (altimetry, gravimetry, in-situ). For each component, we estimate the variance mean over the period 2009-2015, presented in Table 6.

These values will be used to characterize the uncertainty of observability. This has been modeled as a correlated effect with a correlation duration of 6 months. The resulting observability uncertainties will be added to the instrumental uncertainties of each component to compute the covariance matrices. These matrices will then be used in the objectively constrained approach to compute the SLB detailed in section 5 of the PVIR ([AD1]).

The variance of the barystatic sea level is considerably smaller than that of the other components, thus it will not be included in the analysis.

Table 6 *Variance mean over period 2009-2015 of synthetic component*

Component	Relative sea level	Steric sea level	Barystatic sea level
Variance mean (mm²)	0.4	0.6	0.6e-3

Comments

We can observe on Fig.11 and Figure 16 that the synthetic components show an effect temporally correlated over several years or linearly correlated on the relative and steric sea level. The question is then to distinguish whether these are linked to errors in the observation system, in which case it may be appropriate to propose a correction, or whether it is an uncertainty that needs to be prescribed in the uncertainty budget linked to the observability of the system.

To propose a correction of this potential error, it might be possible to adjust a model (order 2 polynomial) that will fit the low frequency signal detected (black solid line on the figures) and would be corrected directly on the real data. This low frequency signal could be considered as systematic errors of the observing system that is why we might propose a correction for it. Then the residuals between the model adjusted and this low frequency signal could be modelised on the observability uncertainties of each component.

However, the time period of the study is for now too low (only 7 years) and these results would need a longer time period to be more robust.

5.1.1. Sea level budget

It is also possible to compute the SLB residuals from OCCIPUT at observation locations (synthetic data) over the period 2009-2015 and make a comparison to the residuals from the observed data used in the project (see Figure 19). To remind, the budget residuals are computed following the equations:

$$R = \Delta GMSL_{rel} - \Delta GMSL_{bary} - \Delta GMSL_{thermo}.$$

Equation 7

We can observe a very good agreement between the 2 time series of the residuals which confirms the interest of this study since the observed behavior of synthetic data seems very close to what is observed with real data. We can also note that the 2 residuals show a similar positive trend of 0.6 mm/yr, the residuals from the synthetic data show more important short time correlated signals. The synthetic residuals have a standard deviation of 2.13 mm whereas the observed data residuals is 1.5 mm.

This preliminary result suggests a potential systematic error in observed sea level budget and therefore its residuals, possibly originating from the combined observational approach utilising altimetry, gravimetry, and in-situ profile data. To mitigate this potential systematic error, further investigations will be needed. While these preliminary results offer valuable insight, their robustness requires validation through several complementary analyses. Replicating this analysis using alternative ocean models with different underlying physics and data assimilation schemes would provide a crucial comparative assessment. Furthermore, extending the temporal scope of the analysis on longer periods would help to discern whether the observed trend persists over time and across different climate variability patterns. Such in-depth validation is essential to confidently attribute the residual trends and develop effective correction strategies.
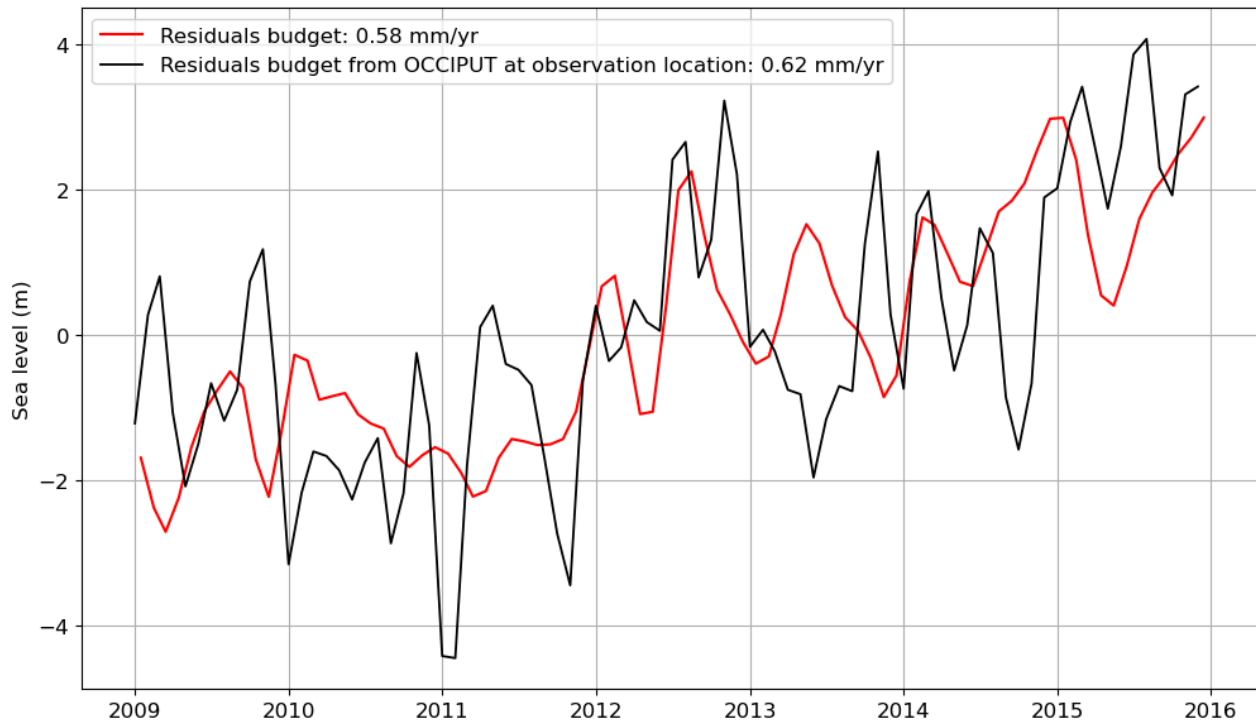
Figure 19 *SLB residuals from OCCIPUT at observation location (black curve) and SLB residuals from observed data (red curve) over the period 2009-2015. A 3-months temporal filter is applied*

5.2. At regional scale

The same approach has been applied at a regional scale; it consists of computing the SLB from the synthetic data to evaluate the uncertainties coming from the observing system. Each synthetic component of the SLB is computed following the procedures described in the ATBD section 2.10.3 and the residuals are computed following equation Equation 7.

Then the trend residuals over the period 2009-2015 are presented in Figure 20. We can observe in these residuals that there are large trends in almost all the oceans. The most important trends are located in areas of strong oceanic currents (Southern Ocean, in the Kuroshio, and Gulf Stream regions). Moreover, we can observe large-scale patterns in almost every region, especially in the Tropical Pacific basin and in the North Atlantic.

These results tend to show even if it was something already expected at regional scale (while not expected at global mean), the observing system is not sufficient to close the SLB regionally regarding its spatial and temporal resolution implied by the resolutions of each component (altimetry, gravimetry and in-situ profiles). It also shows that even if instrumental uncertainties were neglected because they had become too low (thanks to future improvements) it would remain residuals at regional scale due to differences in ocean observability between different systems with

important residuals trends. An effort must therefore be made on the improvement of the knowledge of these observing uncertainties at regional scales in future activities.
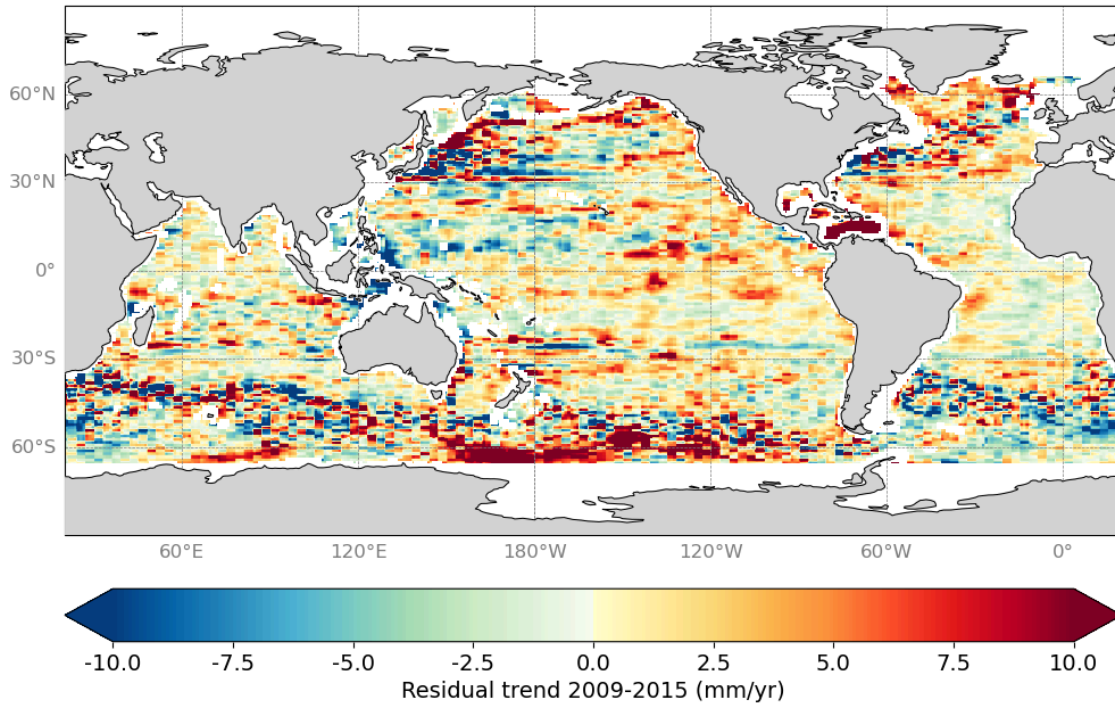

Figure 20 *Sea level budget residual trend from synthetic data over period 2009-2015 in mm/yr*

To date, the evaluation of the regional uncertainties of the observing system has not been performed. One of the objectives would be to determine the spatial scales and temporal scales at which the effective resolution of the observing system is sufficient to close the SLB. These results would provide important information to each component of the SLB to indicate its limitations and improvements that could be made.

These regional uncertainties of the observing system will therefore be used to estimate the SLB at regional scales using the objectively constrained approach (cf section 5.2 of the PVIR).

6. Conclusions and Recommendations

Within the framework of the SLBC_cci+ project, an important effort was made on the different components of the sea level budget to improve and provide robust uncertainty assessment. This was performed by characterising the measurement uncertainties on the different components thanks to a precise analysis on the effect due to the processing and algorithm applied on the data. These measurement uncertainties must continue to be characterized in the future.

For the altimetry and the gravimetry data, an effort has been made to characterise these uncertainties in the form of an uncertainty budget where each contribution to the uncertainties has been identified and described properly (linear time correlated effect, correlated or uncorrelated effect) with a standard uncertainty value. This approach therefore allows to construct variance covariance matrices for any time scale and time period.

For the steric component and the different mass component, these measurement uncertainties have been modeled by estimating a standard deviation, even if this information is crucial for the uncertainty assessment activities, it cannot be used to describe correlated effects affecting uncertainties. An effort must be made into the future to improve the uncertainty knowledge on these components in order to estimate the correlated uncertainty.

These uncertainties have been used for the computation of the sea level budget and its residuals by summing the different uncertainties on the components (as each observing system is considered independent from the other ones). Over the period 2002-2016, the residuals trend of the SLB are estimated to 0.33 +/- 0.43 mm/yr when using the gravimetric data and 0.74 +/- 0.3 mm/yr when using mass components.

Furthermore, for the first time the uncertainties have also been estimated at regional scale also in the form of an uncertainty budget (which in this case is location dependent) for the altimetry and gravimetry. These uncertainties have been used to estimate the regional trend uncertainties on the different components as well as the regional SLB residuals.

For the first time, activities have also led to breaking down SLB uncertainty into two sources; measurement uncertainties due to errors and approximations within each individual observing system. Represents potential for improvement through better instruments/algorithms. Structural uncertainty due to the effective resolution differences between observing systems (Argo, GRACE, Altimetry) which represents the inherent observability with the current system, will be estimated with synthetic data.

The estimation of the structural uncertainty has been made using synthetic observations from the OCCIPUT ocean model. An important result of this activity that has been discovered is that there could be potential large-term time-correlated structural errors that are affecting some observing system (mostly altimetry and in-situ) that could lead to explain the non-closure of the SLB over period 2009-2015. More in depth analysis would be necessary to consolidate this major result particularly over a longer time period. If this result proves robust, it would imply the need to propose a correction to these systematic errors on the budget computation.

End of the document